Unhealthy and out of shape: Deciphering the slow response of glaciers to climate change

Master Thesis

Author(s):
Wettstein, Christian Alexander

Publication date:
2023-07

Permanent link:
https://doi.org/10.3929/ethz-b-000627231

ETH
Eidgenössische Technische Hochschule Zürich
Swiss Federal Institute of Technology Zurich

D ERDW
EARTH SCIENCES

Master Thesis

Unhealthy and out of shape: Deciphering the slow response of glaciers to climate change

Submitted at the Dept. of Earth Sciences at ETH Zurich

Conducted at the Dept. of Civil, Environmental and Geomatic Engineering

Institute of Hydraulics, Hydrology and Glaciology (VAW)

Supervised by

Dr. Harry Zekollari

Prof. Dr. Daniel Farinotti

Prof. Dr. Hansruedi Maurer

Submitted by

Christian Wettstein

17-929-837

July 2023

Abstract

Ongoing climate change has resulted in substantial glacier volume loss worldwide. Due to their slow adjustment to temperature changes, glaciers are largely in imbalance with the current climate. Hence, they reflect a mixture between past and current climate variability combined with anthropogenic forcing. Due to this delayed response, glaciers in the European Alps will for instance lose 50% of their mass by 2050, largely irrespective of the climate scenario. The retreat of glaciers has a severe impact on sea level rise, water supply, natural catastrophes like glacier lake outburst floods, hydro-electricity production and tourism. Therefore, predicting the future retreat for glaciers is of great importance in order to quantify the effect of climate mitigation measures and to perform adequate risk management. A widely accepted method to assess the response time of these ice masses is to rely on the e-folding time. This is the time it takes for a glacier to complete 1-e^{-1} (=63%) of its volume/area change from an initial state to a perturbed one.

In this study, the regional e-folding time is examined for all regions belonging to the Randolph Glacier Inventory, which divides the Earth into 19 distinct regions based on glacier coverage. This e-folding time is calculated from GlacierMIP3 experiments, in which different glacier models simulated the advance or retreat for various climate scenarios over multi-millenial time scales. This long time horizon allows glaciers to reach a state of equilibrium which contrasts with current approaches from the literature, where glacier loss is typically only simulated until the end of the century, a time scale over which these ice masses are far from steady state.

Simulations from eight different glacier models indicate that the most important parameter to describe the regional response time is the region's mean slope. Areas with a mean slope below 13% yield an e-folding time far greater than 100 years, whereas steeper regions suggest faster e-folding times below 100 years. In case of a 75% relative volume loss (between current state and final steady state volume), the Low Latitude region adapts to warming the fastest with an e-folding time of 10.8 $\pm$ 1.0 years. In contrast, the Russian Arctic corresponds to the slowest region for the same volume loss scenario, with an e-folding time of 281.4 $\pm$ 88.5 years.

The examined models in GlacierMIP3 are based on different glacier-modelling methods to simulate the mass balance and the resulting advance or retreat. Half of the models follow a volume-area scaling approach in which ice flow is neglected, while the others incorporate these ice dynamics. We found that volume-area scaling models generally yield faster e-folding times than the ones accounting for ice flow, with GLIMB being an exception. In fact, GLIMB produces the slowest e-folding times throughout all models, despite being based on a volume-area scaling approach. This slow response could partially be due to the representation of the mass balance in GLIMB, which includes additional climate forcing parameters versus other models that typically only rely on temperature and precipitation as input.

Contents

1 Introduction

The impact of current climate change has led to a significant decline in glacier volume. In the past, glaciers have always adjusted to natural climate fluctuations. However, the fraction of anthropogenic global glacier mass loss between 1991 to 2010 increased from 25% to 69% compared to the proportion between 1851 and 2010 (Marzeion et al., 2014). When these ice masses retreat, they can lead to destabilization of slopes, the creation of landslides and rockfalls and the formation of natural dams which pose an imminent danger for water outbursts (Compagno, 2022; Veh et al., 2020). Since glaciers have become important touristic destinations throughout the last decade, their economical value has substantially increased (e.g. Fischer et al., 2011; Welling et al., 2015). Moreover, they act as a crucial source of melt water during dry seasons, supporting downstream water consumption and agriculture (e.g. Biemans et al., 2019; Haeberli and Weingartner, 2020; Huss and Hock, 2018). The resulting change in river runoff and formation of natural dams is of interest for producing hydroelectricity (Farinotti et al., 2019; Milner et al., 2017; Patro et al., 2018; Schaefli et al., 2019) in order to transition to a renewable energy source. However, the increased runoff also directly contributes to rising sea levels (Edwards et al., 2021; Marzeion et al., 2020). Glaciers (here: glaciers which are distinct from the Greenland and Antarctic ice sheets) account for less than 1% of the total ice mass (IPCC, 2013) and are estimated to hold a volume equivalent to a 0.3-0.4m increase in sea level (Farinotti et al., 2019; Huss & Farinotti, 2012). Although this may seem relatively small compared to the 65m sea level potential in the ice sheets, glaciers are currently the primary contributors to the sea level increase and are expected to remain so in the near future (IPCC, 2021). Their significant contribution is the result of glaciers having a shorter response time compared to ice sheets. Glaciers are assumed to adapt to changing climatic conditions within decades to centuries (Christian et al., 2018; Marzeion et al., 2014; Zekollari et al., 2020), whereas ice sheets can take up to thousands of years to adjust (Cuffey & Paterson, 2010).

Since glaciers are subject to a response time when adapting to new climate conditions, the present-day glacier retreat is a mixture of past and current climate variability combined with anthropogenic forcing (Marzeion et al., 2014; Zekollari et al., 2019). For instance, by 2050 a volume loss of 50% for European alps is estimated, largely irrespective of future climate (Zekollari et al., 2019). It is only in the second part of the 21st century, that this loss strongly depends on the projected climate perturbation (Zekollari et al., 2019). Furthermore, the relative volume change and the time scales over which this occurs can significantly vary among glaciers, even if they are close to each other. This is primarily due to variations in their geometry and local climatic conditions, including precipitation patterns (Schuster, 2020).

Thus, understanding how glacier dominated regions react to climate change and quantifying their response time is a crucial step in predicting future glacier evolution, thereby informing policy-making efforts and allowing to perform risk mitigating measures.

2 Background

2.1 Characteristics of a glacier

A glacier consists of an accumulation and an ablation area, as shown in Fig. 1. In the accumulation area, snow gets compressed and transformed into ice within decades to centuries (Cuffey & Paterson, 2010). This region is characterized by a positive annual net mass balance. The gravitational force causes the accumulated ice to flow downstream into the ablation zone. Due to melting, this area is dominated by a negative mass balance. The boundary between the accumulation and the ablation zone is defined as the equilibrium line altitude (ELA), in which the annual mass balance is equal to zero (see Fig. 1). This behaviour is usually described by the mass balance gradient, which corresponds to the derivative of the mass balance with respect to the height. Since the mass balance is given in unit mm w.e. yr^{-1}, the mass balance gradient is in mm w.e. $\mathrm{yr}^{-1}\mathrm{m}^{-1}$. A large mass balance gradient is characterized by strong accumulation and ablation above and below the ELA, which results in a large mass transfer between the two sections in order to maintain a steady state profile (Hooke, 2019).
The stresses exerted by gravity on ice induce deformation called strain ϵ. The rate at which these stresses are acting from different directions on a glacier is called strain rate $\dot{\epsilon}_{ij}$ (Hooke, 2019). As the strain rate is dependent on all three dimensions, the effective strain rate $\dot{\epsilon}_e$ is often used (Hooke, 2019; Schuster, 2020). This effective strain rate is defined by Glen's flow law (Glen, 1955):

$$\dot{\epsilon}_e = A\sigma_e^n, \tag{1}$$

where A corresponds to the ice creep parameter, σ_e to the effective shear stress and n to the ice creep exponent. The ice creep parameter describes the viscosity of a medium and is dependent on temperature, water content of ice, pressure, texture fabric and impurities (Hooke, 2019). The creep exponent depends on the creep mechanism (e.g. dislocation creep, diffusion creep) and is usually set to 3. Equation (1) is used to describe the glacier flow in numerical models, where the stress (σ_e^n) can be calculated from the full stress balance (Full-Stokes) or simplified version thereof (e.g. shallow ice approximation).

Over time, glaciers adapt to climate oscillations by advancing or retreating at a pace, which is determined by the glacier's response time. Quantifying and characterizing the response time of a glacier is an area of ongoing research, and various methods can yield different results. In this thesis, we categorize the existing methods into three main categories: (i) semi-analytical response time, (ii) simplified numerical models and (iii) numerical models accounting for ice dynamics.

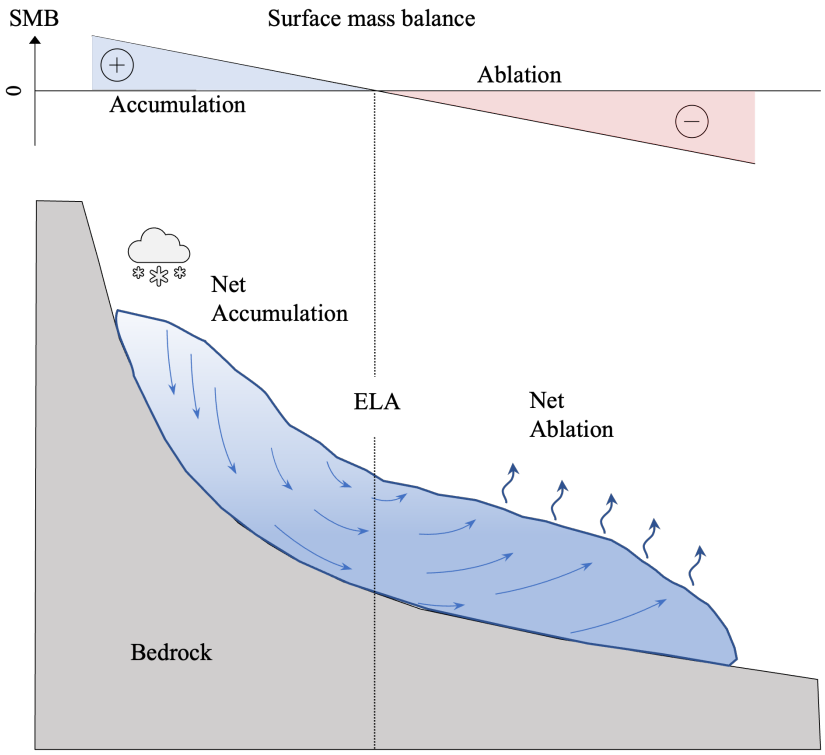

Figure 1: Schematic of a glacier with its subsections and corresponding mass balance. Snow precipitates in the accumulation zone where it gets transformed into ice, leading to a positive surface mass balance (SMB). Gravitational pull leads to downward ice flow into the ablation zone, in which melting occurs, resulting in a negative SMB. Both areas are separated by the equilibrium line altitude (ELA).

2.2 Response time of glaciers

2.2.1 Semi-analytical response time

An early method for analyzing the response time of climatic adjustments was introduced by Nye (1965), where a linearized equation for ice flow based on kinematic wave theory was used (Oerlemans, 2007). By neglecting diffusion, this approach, however, resulted in a significant underestimation of the actual response time. A practical approach was provided by Jóhannesson et al. (1989), where the volume response time τ_v is calculated as the ratio between a characteristic ice thickness H^* and the ablation b_t at the glacier tongue:

$$\tau_{v,jo} = \frac{H^*}{-b_t} \tag{2}$$

A flowchart overview of this method is provided in Fig. 2. The approach is based on estimating the time required for a glacier to transition from one geometry to another, given the mass balance conditions (Oerlemans, 2007). However, while Equation (2) yields good results for steep glaciers, it has a tendency to underestimate the time needed for adjustment for gentle slopes (e.g. Harrison et al., 2003; Oerlemans, 2007; Oerlemans, 2001; Zekollari and Huybrechts, 2015). Moreover, selecting the appropriate ice thickness H^* poses challenges as it significantly

impacts the result. Often, the maximum ice thickness is used, but this approach may not always be representative of the glacier's overall characteristics (Zekollari & Huybrechts, 2015). Nevertheless, the method by Jóhannesson et al. (1989) has been extensively used to explore glacier responses to climate perturbation (e.g. Christian et al., 2018; W. Harrison et al., 2001; Oerlemans, 2007; Oerlemans, 2001; Roe and O'Neal, 2009).

Many analytical or scaling approaches such as Equation (2) assume that glacier area and length respond instantaneously to volume changes (Schuster, 2020) without considering the influence of ice flow (arrows in Fig. 1). This oversight is significant because ice flow is a crucial component of the dynamic response of glaciers to changing climatic conditions. Because these models assume instantaneous adjustment (corresponding to $n = \infty$, in Glen's law, Equation 1) they are commonly referred to as one-stage models (Roe & Baker, 2014). Under this assumption, deformation does not occur below a specific threshold, meaning that the ice does not flow. Above, ice deformation takes place at a rate where the stress does not surpass a certain threshold (Hooke, 2019; Schuster, 2020). Hence, these one-stage models tend to underestimate the response time compared to higher-stage models or when using a numerical flowline model (Schuster, 2020). Two-stage models, which consider a time delay between volume and area change, were developed by Harrison et al. (2003) and Lüthi (2009). While the former follows an analytical approach, the latter solves the governing equations numerically. The three-stage model, which is also solved numerically, involves the calculation of mass distribution from the interior to the terminus of the glacier in three overlapping stages: First, the mass balance perturbation leads to a change in interior thickness, which drives the change in terminus ice flux and thereby, resulting in glacier length change (Schuster, 2020).

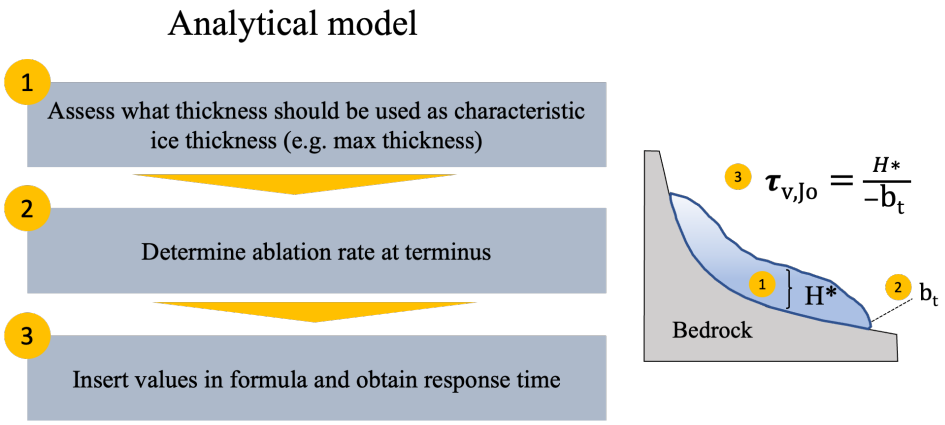

Figure 2: Schematic flowchart of widely used analytical approach by Jóhannesson et al. (1989).

2.2.2 Simplified numerical models

In the scientific literature, the e-folding timescale is commonly used to determine the response time from numerical experiments. This e-folding time represents the duration it takes for a glacier to complete approximately $1 - e^{-1}$(i.e. 63.2%) of the total volume or area change with respect to specific climate perturbations or forcing (e.g. Leysinger Vieli and Gudmundsson, 2004; Oerlemans, 2018; Zekollari et al., 2020). The concept of the e-folding time is more extensively discussed in Section 2.3.

Here, we provide an overview of different numerical models used to simulate the large-scale evolution of glaciers, since these are the types of approaches that participated in the third phase of the Glacier Model Intercomparison Project (GlacierMIP3), which are the main data source for the analysis in this thesis (detailed in Section 3.1).

In previous studies, various numerical methods with simplified models have been utilized to assess changes in glacier volume change at large spatial scales (regional to global). The majority of these methods calculate the transient surface mass balance directly using the degree-day method (Bliss et al., 2014; Hirabayashi et al., 2013; Huss & Hock, 2015; Marzeion et al., 2012; Maussion et al., 2019; Radić & Hock, 2011; Rounce, Hock, & Shean, 2020). This method determines the daily melt by multiplying a coefficient with the difference between the mean daily temperature and a base temperature, which is typically set to zero degrees Celsius (NRCS, 2009):

$$M = C_m(T_a - T_b), \tag{3}$$

where M corresponds to the snowmelt, C_m to the degree-day coefficient (often with a distinction for snow- and icemelt to represent different albedo), T_a to the mean daily air temperature and T_b to the base temperature.

In modelling glacier evolution, the majority of these approaches neglect the glacier geometry (ice thickness distribution) and use scaling relations such as volume-area scaling or volume-length scaling to represent the glacier volume and its temporal changes (Huss & Hock, 2015). Moreover, these models often disregard changes in surface elevation, although incorporating such changes would be crucial to accurately capture elevation-mass-balance feedbacks in glacier modelling (e.g. Huss and Hock, 2015; Oerlemans et al., 1998). In the left part of Fig. 3, an overview of the required steps for such volume-area scaling models is given.

The Global Glacier Evolution Model (GloGEM), developed by Huss and Hock (2015), represents a more advanced approach compared to the previously mentioned models. It explicitly considers the glacier's geometry by incorporating distributed ice thickness information. Additionally, GloGEM accounts for certain complexities of glaciers, such as changes in surface elevation and frontal ablation in marine-terminating glaciers. GloGEM obtains the outline of a specific glacier from the Randolph Glacier Inventory (RGI), which was developed by Pfeffer et al. (2014) in order to standardize representation in e.g. modelling studies. The ice thickness is reconstructed by Huss and Farinotti (2012). In GloGEM, the glacier is divided into various elevation bands. Within each band, the mass balance is computed on a monthly basis. Following each mass-

balance year, adjustments are made to the thickness, surface elevation, and extent of the glacier. This redistribution of mass change across all elevation bands follows an empirical function. This function assumes no elevation change at the highest point of the glacier and maximum change at the glacier's tongue (Huss & Hock, 2015). This height-dependent redistribution aligns with observations from retreating glaciers, where the most significant changes in mass are observed near the glacier terminus (Arendt et al., 2002; Huss & Hock, 2015; Jóhannesson et al., 1989). However, GloGEM neglects the incorporation of ice dynamics which is why an extended version has been developed, described in Section 2.2.3. A flowchart of GloGEM is shown on the right part of Fig. 3.

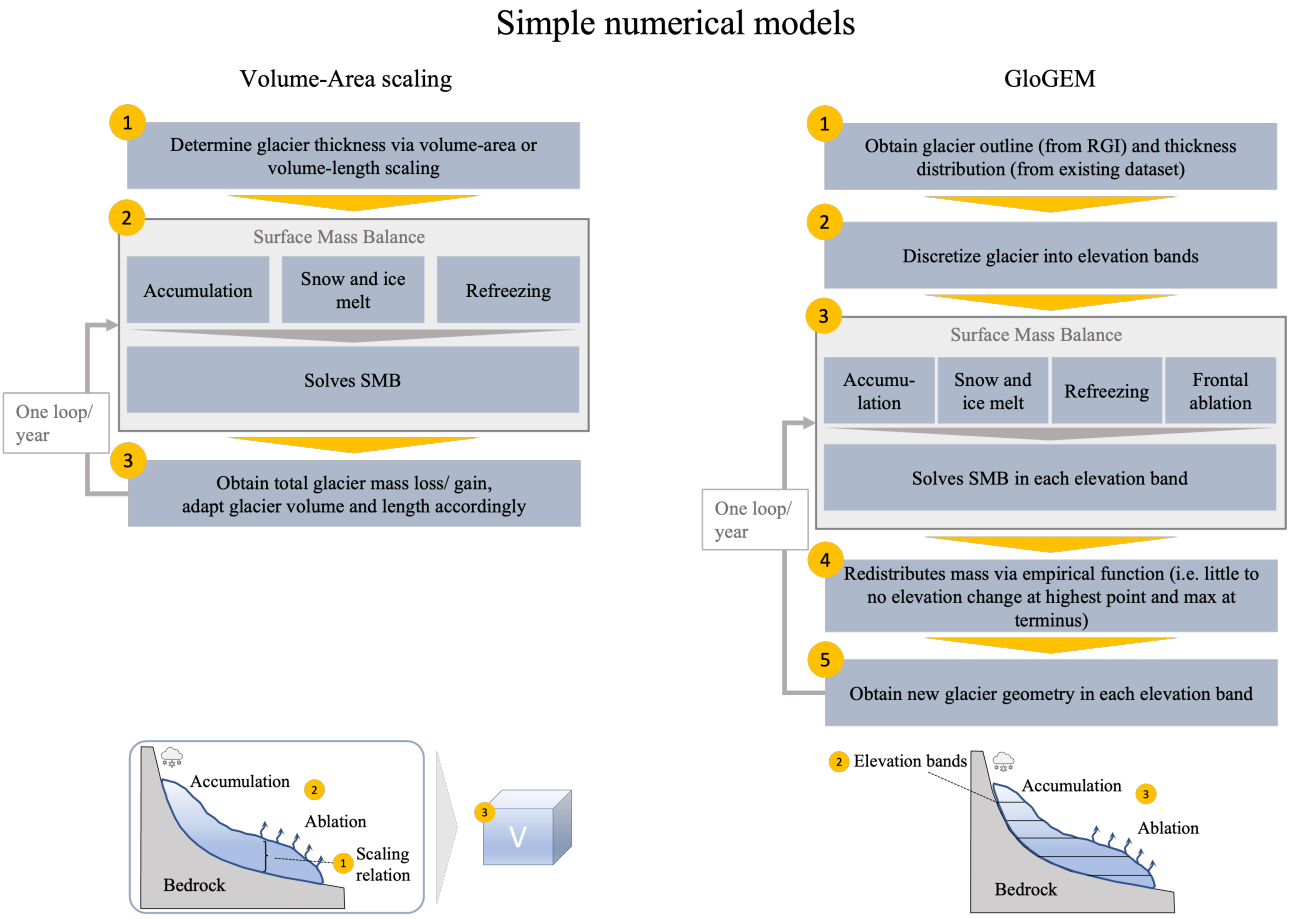

Figure 3: Flowchart of simple numerical models. Left chart shows the required steps a volume-area scaling approach uses. Right shows the required steps in GloGEM to obtain the new glacier geometry.

2.2.3 Numerical models accounting for ice dynamics

GloGEMflow, an extended version of GloGEM, has been developed by Zekollari et al. (2019) to incorporate an ice flow component. This approach is discussed in more detail because an important part of this thesis' response time analysis is based on simulations with this model.
GloGEMflow consists of two components: The surface mass balance component from GloGEM and the ice flow component, which, combined lead to the temporal evolution of a glacier (Zekollari et al., 2019). The ice flow is incorporated by using the Shallow-Ice approximation (SIA) (Hutter, 1983) and assuming a basal shear (σ_b) which is proportional to the local ice thickness H and surface slope $\frac{\partial s}{\partial x}$ (Zekollari et al., 2019):

$$\sigma_b = -\rho g H \frac{\partial s}{\partial x}, \tag{4}$$

where g is the gravitational acceleration and ρ the ice density.
Subsequently, Zekollari et al. (2019) describe the mass transport through a Glen (1955) type of flow law (see Equation (1) for Glen's flow law), in which the depth-averaged velocity $\overline{u}$ is defined as:

$$\overline{u} = \frac{2A}{n+2} \sigma_b^n H, \tag{5}$$

where n and A correspond to the Glen's flow law exponent and deformation-sliding factor respectively.
The glacier geometry is then updated in every simulated time step through the continuity equation:

$$\frac{\partial H}{\partial t} = \nabla \cdot f + b, \tag{6}$$

where b represents the SMB and $\nabla \cdot f$ the local divergence of the ice flux, i.e. $f = D\frac{\partial s}{\partial x}$. Here, D represents the diffusivity factor. A flowchart overview of the simulated steps with GloGEMflow is given in Fig. 4.
The Open Global Glacier Model (OGGM), developed by Maussion et al. (2019), is another numerical model that incorporates ice flow dynamics. The core concept is very similar to GloGEMflow. It also utilizes the SIA (Equation 4) in order to obtain the depth-averaged velocity (Equation 5) and is based on a coupled SMB ice flow model.

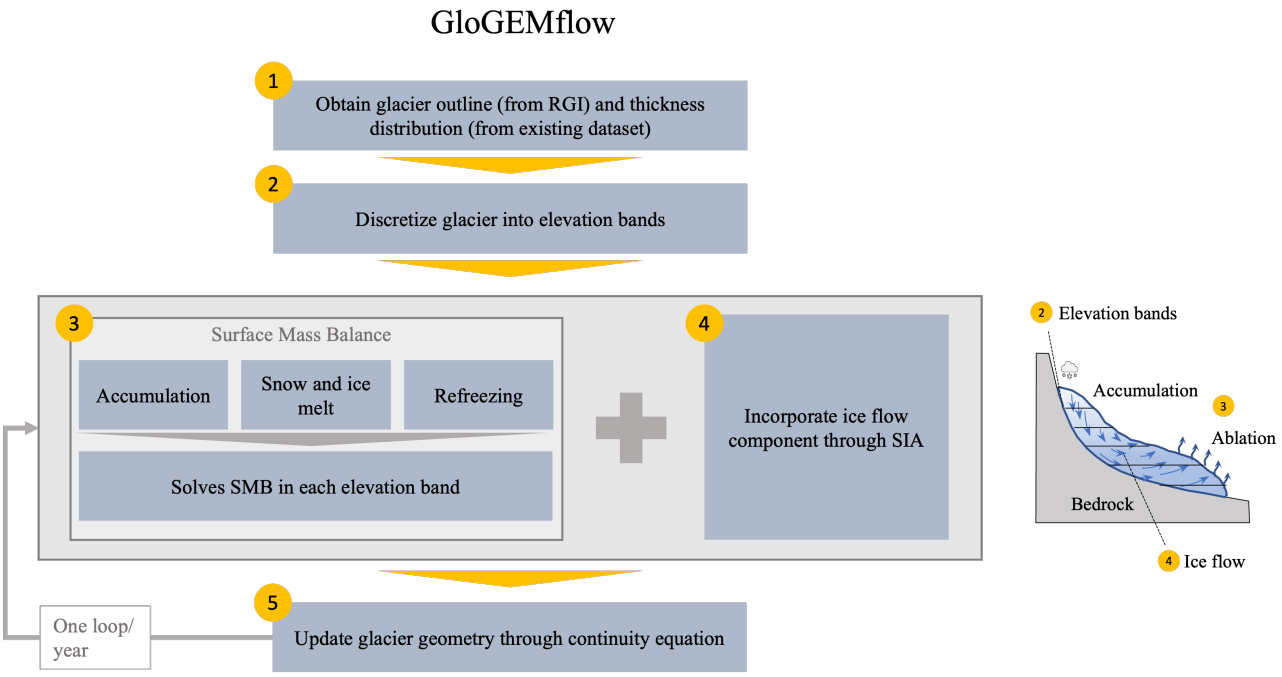

Figure 4: Flowchart of GloGEMflow which incorporates ice dynamics.

2.3 Concept of the e-folding time

As briefly discussed in Section 2.2.2, the e-folding time is commonly used to express the response time from numerical experiments and defined as the time it takes for a glacier to complete $1-e^{-1}$ (ca. 63.2%) of its volume/area change from an initial state to a perturbed one. Fig. 5 provides a schematic representation of how this time is derived. In case of increased precipitation, i.e. increase in mass balance, a glacier advances and increases in size. As can be seen in the figure, this advance starts rapidly and eventually slowly converges to a new steady state volume. The corresponding e-folding time for this positive mass balance forcing is marked as τ_+. During a decrease in precipitation, i.e. decrease in mass balance, the glacier retreats and shrinks in size. This response time τ_- is usually faster than for glaciers with an increase in precipitation (i.e. $\tau_- < \tau_+$).

2.4 Concept of the stabilization time

Another approach of characterizing the response of glaciers to climate change is by determining the time it takes for a glacier to fully reach its steady state, hereby referred to as the stabilization time. Fig. 6 provides a schematic representation of how this stabilization time is derived. For both increase and decrease in precipitation, the stabilization time is located where the change in relative volume has become very small, i.e. a state of equilibrium has been reached. The same behaviour as for the e-folding time is visible, where a glacier usually reaches its stabilization time faster in a climate scenario with decreasing precipitation.

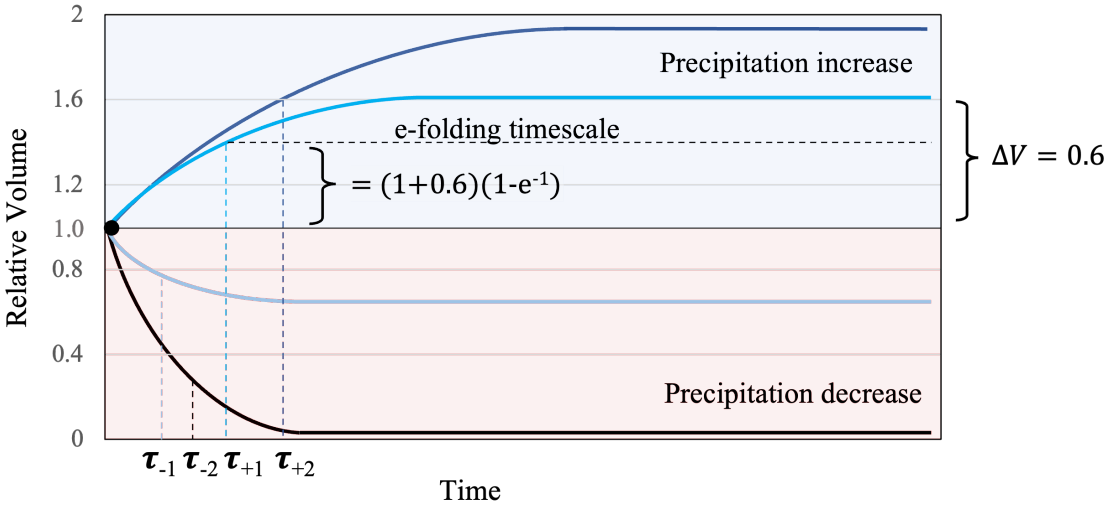

Figure 5: e-folding time $\tau_{+1,2}$ for an increase in precipitation, i.e. increase in mass balance (often associated with cooling) and $\tau_{-1,2}$ for a decrease in precipitation, i.e. decrease in mass balance (often associated with warming). The e-folding timescale represents the time a glacier needs to complete $1 - e^{-1}$ i.e. 63.2% of the total change. In general, glaciers adjust to a negative mass balance faster than to a positive one, resulting in $\tau_+ > \tau_-$.

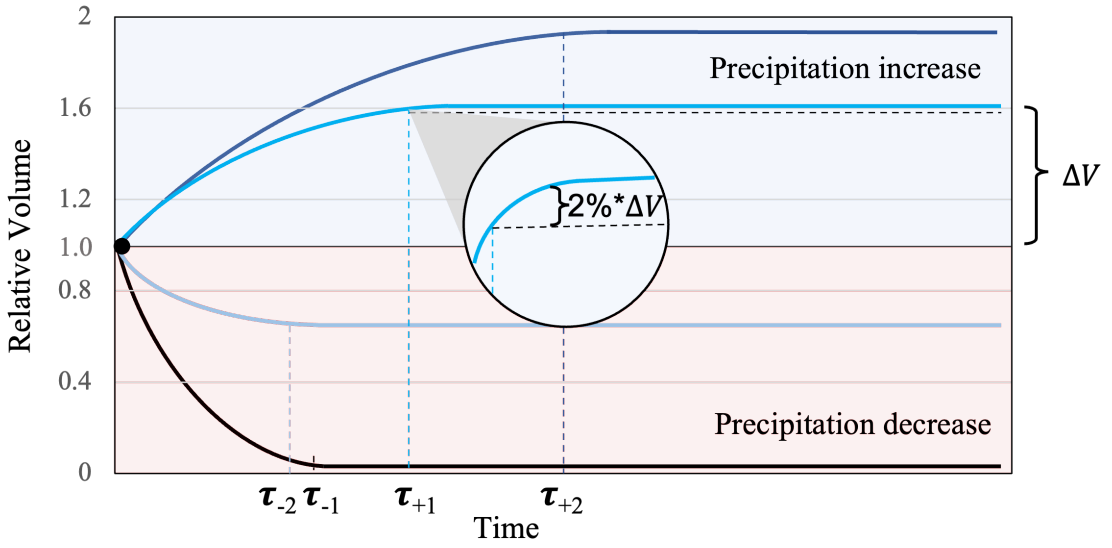

Figure 6: Stabilization time $\tau_{+1,2}$ for an increase in precipitation, i.e. increase in mass balance (often associated with cooling) and $\tau_{-1,2}$ for a decrease in precipitation, i.e. decrease in mass balance (often associated with warming). The stabilization time corresponds to the time a glacier needs to fully reach its steady state. In general, glaciers adjust to a negative mass balance faster than to a positive one, resulting in $\tau_+ > \tau_-$.

3 Methodology

This study's method is divided into five sections. Section 3.1 provides an introduction on the global glacier mass change equilibration simulations, on which this thesis' results are built upon. In Section 3.2, the different glacier models used for these equilibrium simulations are introduced. The filtering process for retrieving the response time from the glacier experiments is described in Section 3.3, followed by the calculation of the e-folding time in Section 3.4. Finally, section 3.5 focuses on setting up a random forest algorithm for response time prediction, which is utilized to analyze key parameters that influence the e-folding time of glaciers by examining the structure of the decision tree.

3.1 Global glacier mass change equilibration experiments

GlacierMIP3 represents the third phase of the GlacierMIP series, which was designed to provide a framework for a coordinated comparison of global-scale glacier mass change as part of the World Climate Research Project. The setup process of GlacierMIP3 can be divided into three steps [1]. First, participants extracted the glacier geometry from the Randolph Glacier Inventory (RGI). Next to providing information about the glaciers' geometry, the RGI also subdivides the world into different regions, displayed in Fig. 7 and Table 1. In a second step, various climate conditions were repeatedly imposed over multi-millennia time scales using data from CMIP6 Global Circulation Models (GCMs). This extended time horizon enables the glaciers to stabilize under specific climatic conditions (e.g. in a +2 degree world), which contrasts with the classic 2100 time horizon that is typically considered in glacier modelling studies, and in which glaciers are subject to changing climatic conditions throughout the 21st century (where by 2100 the glaciers are typically still far from equilibrium with the imposed climatic conditions). CMIP6, the sixth phase of the Coupled Model Intercomparison Project, uses climate models from various research groups worldwide in order to project future climate evolution under various scenarios. The input models take chemistry, biosphere and their interplay with land, oceans and ice into account and have undergone significant improvements in the last decade (Hausfather, 2019). Therefore, the resulting projected climate scenarios of CMIP have become essential to the Intergovernmental Panel on Climate Change (IPCC) and other international climate assessments (WCRP, 2022). GlacierMIP3 participants used five different GCMs for the experiments from which the modelled climate data was then continuously repeated. Moreover, three projected climate scenarios, namely SSP-126, SSP-370 and SSP-585 were used. The characteristics of these scenarios are briefly discussed in Table 2. In the third and final step, the equilibrium of glaciers was simulated using climatic forcing from eight distinct repeat periods, as outlined in Table 3. To avoid cyclicity in volume or area time series, the years within these periods were shuffled.

[1] GlacierMIP3 set up is described in detail on the project's Github: https://github.com/GlacierMIP/GlacierMIP3/blob/main/GlacierMIP3_protocol.md#section-6

In total, 80 experiments per participant and per RGI region were conducted (see Fig. 7 and Table 1 for RGI region overview) : 5 GCMs for 4 historical time periods (i.e. 20 simulations, Table 3, first row) and 5 GCMs for 4 projected time series and 3 SSP scenarios (i.e. 60 simulations, Table 3, second row).

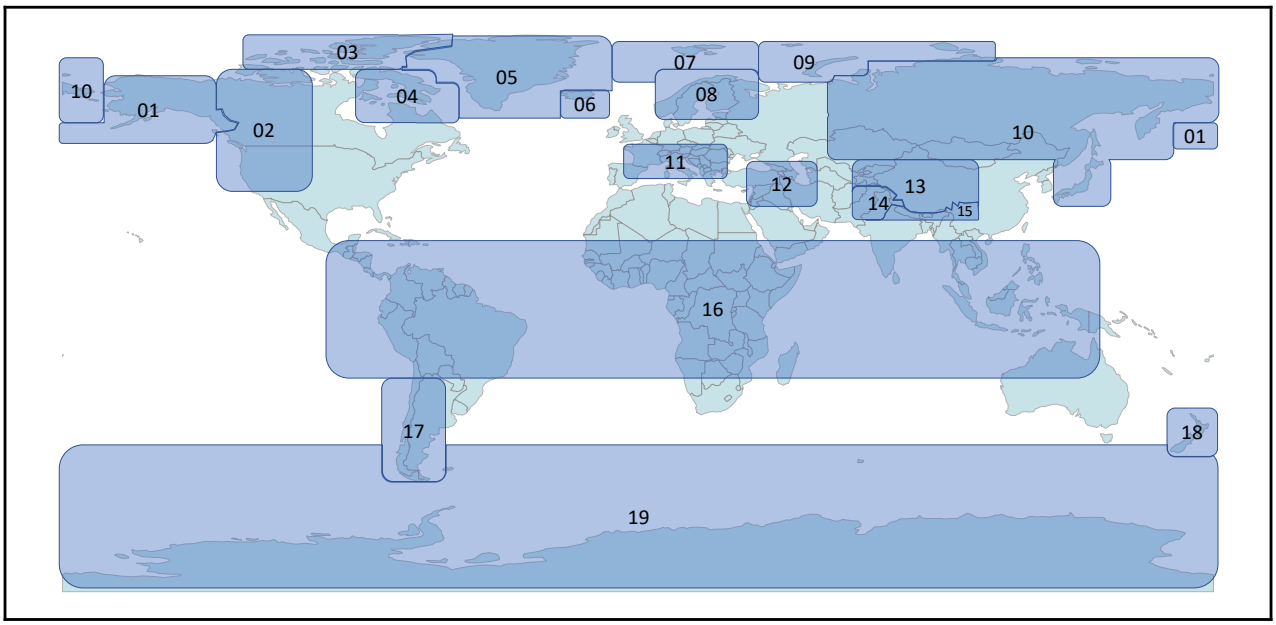

Figure 7: Map of the 19 RGI regions with their corresponding names displayed in Table 1. A region which has been simulated by a GlacierMIP3 participant results in 80 experiments. Outlined regions and names are adapted from the Randolph Glacier Inventory and underlying map obtained with the geopandas library in python, developed by Jordahl et al. (2020).

Table 1: RGI regions which are used to describe Fig. 7.

Number	Region name	Number	Region name
01	Alaska	11	Central Europe
02	Western Canada and United States	12	Caucasus and Middle East
03	Arctic Canada North	13	Central Asia
04	Arctic Canada South	14	South Asia West
05	Greenland Periphery	15	South Asia East
06	Iceland	16	Low latitudes
07	Svalbard	17	Southern Andes
08	Scandinavia	18	New Zealand
09	Russian Arctic	19	Antarctic and subantarctic
10	North Asia		

Table 2: Three different SSP Scenarios used in GlacierMIP3 simulations.

Scenario	**Radiation increase by 2100**	**Description** (Boettinger & Kasang, 2021)
SSP-126	2.6 W/m^2	Optimistic scenario, which simulates future development within the 2°C target.
SSP-370	7 W/m^2	Scenario which displays the medium to high end of plausible future pathways.
SSP-585	8.5 W/m^2	Represents upper boundary of scenario ranges described in the literature, also referred to as 'business as usual' scenario.

Table 3: Eight repeat-periods used for climate forcing in GlacierMIP3.

1851-1870	1901-1920	1951-1970	1995-2014
2021-2040	2041-2060	2061-2080	2081-2100

3.2 Models

In this thesis, simulations from 8 different glacier models are used. A short description on each model is given in Table 4. The column *Model name* represents the specific names assigned to each model used in this study for reference and analysis purposes. The *Classification* column provides information on the general approach used by each model, i.e., whether the more complex ice dynamics were implemented or not. The *Description* column describes the specific details of the underlying principle, including the research group responsible for developing the model. The last column mentions the research teams, which performed the simulations used in this thesis.

The models James, GLIMB, OGGM-VAS and Kraaijenbrink follow a volume-area scaling approach with some differences in obtaining the mass balance. While James' and GLIMB's mass balance is based on an energy balance method, OGGM-VAS and Kraaijenbrink utilize the degree day method (see Equation 3). All Models, which incorporate ice dynamics like Rounce, OGGM_v1.6, Compagno and Zekollari follow the degree day method to calculate the mass balance. The latter two, however, do not calculate the mass balance directly but obtain it from GloGEM.

Table 4: Glacier models which provided the simulations used in the thesis. The column *Model name* corresponds to the name the models are referred to in the text as well as in the plots. Table is continued on the next page.

Model name (this thesis)	**Classification** (see Section 2.2 for comparison)	**Description/ Approach**	**Simulations performed by**
Compagno	Numerical model, incl. ice dynamics	Model (GloGEMflow, developed by Zekollari et al., 2019) uses degree day method, incorporates ice dynamics and its mass balance is taken from GLoGEM (Huss & Hock, 2015).	Loris Compagno, Matthias Huss and Harry Zekollari
GLIMB	Volume-area scaling	Model by Sakai and Fujita (2017) is based on an energy balance model to obtain the mass balance.	Koji Fujita and Akiko Sakai
James	Volume-area scaling	Unpublished model which uses a simplified energy balance to obtain the mass balance and is based on Giesen and Oerlemans (2013).	Megan James and Tamsin Edwards
Kraaijenbrink	Volume-area relation per elevation band	Model developed by Kraaijenbrink et al. (2017) is based on mass balance gradient (Benn & Lehmkuhl, 2000) and uses degree day method.	Philip Kraaijenbrink and Walter Immerzeel

Table 4: *Continued Table 4*

Model name (this thesis)	**Classification** (see Section 2.2 for comparison)	**Description/ Approach**	**Simulations performed by**
OGGM-VAS	Volume-area scaling	Model by Marzeion et al. (2012) utilizes the degree day method.	Ben Marzeion and Moritz Oberrauch
OGGM_v1.6	Numerical model, incl. ice dynamics	Mass balance obtained similarly to OGGM-VAS (Marzeion et al., 2012).	Lilian Schuster and Fabien Maussion
Rounce	Numerical model, incl. ice dynamics	Hybrid model between PyGEM (Rounce, Khurana, et al., 2020) and OGGM (Maussion et al., 2019). PyGEM uses degree day method (Equation 3) and OGGM provides ice dynamics (flow lines).	David Rounce
Zekollari	Numerical model, incl. ice dynamics	Model (GloGEMflow3d, unpublished 3d version of GloGEMflow by Zekollari et al., 2019) obtains mass balance from GloGEM (Huss & Hock, 2015).	Harry Zekollari and Matthias Huss

3.3 Data processing

3.3.1 Regional glacier simulations

The research groups described in Table 4 conducted simulations on a per-glacier basis, which resulted in individual glacier volume response time simulations. For each RGI region, all individual glacier simulations were then summed up, resulting in a regional volume response time simulation for that particular region. The left part of Fig. 8 provides an example of the Alaska regional volume response time simulation for one specific climate scenario, simulated with the Compagno model. The right part displays the simulations performed on all climate forcings, which results in 80 simulations per region. These simulations act as foundation for this thesis as all analyses are built upon them.

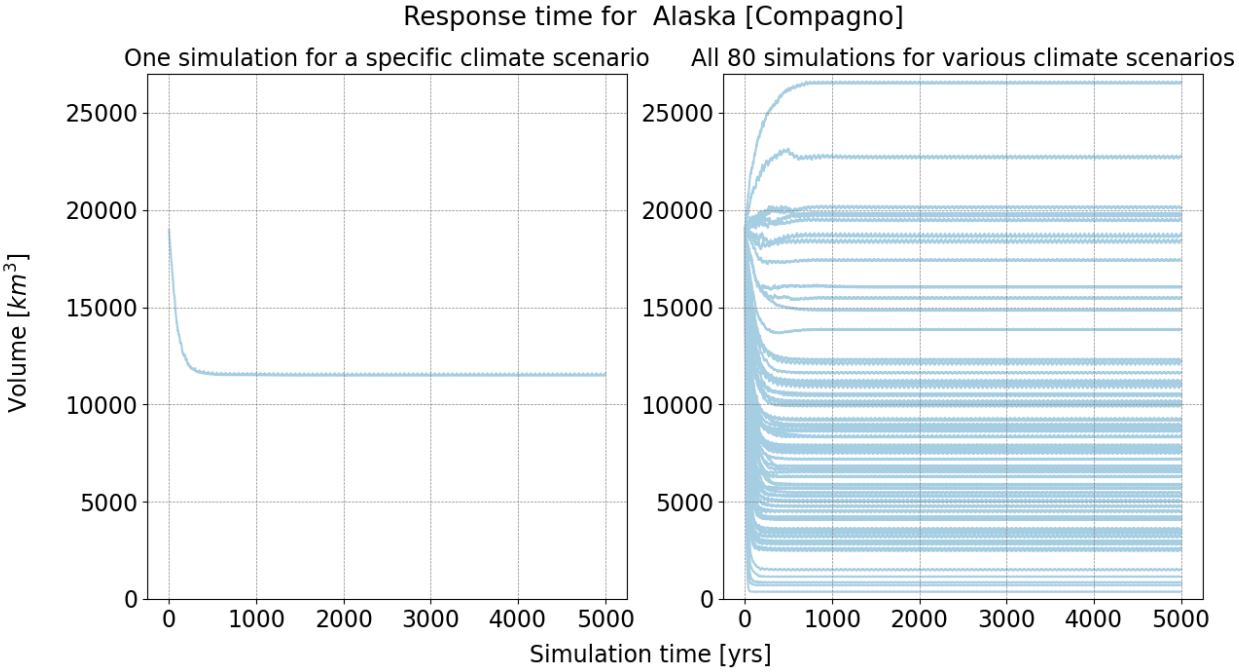

Figure 8: Glacier volume experiments for Alaska simulated with the Compagno model (see Table 4 for a model overview). Left plot shows the regional response time for a specific climate scenario. This is the result of summing up all individual glacier response times for said specific climate scenario. Right plot includes all different scenarios, i.e. shows 80 different simulations.

3.3.2 Filtering process

Filtering out erroneous data or simulations which do not reach a state of equilibrium is crucial as such data can have a significant impact on the calculation of the response time. While the focus in this study is on examining the e-folding time, a different concept of utilizing the stabilization time is investigated in Section 5.4 as well. Therefore, the filtering process between these methods is described here separately as they slightly differ between each other.

Filtering process e-folding time

The filtering process to determine the e-folding time can be divided into three steps:

As described in Section 2.3, the e-folding time is based on the assumption that the volume increase or decrease follows an exponential fit (see Fig. 5). Hence, data which does not adhere to an exponential fit will be removed in a first step. This is done by examining different R^2 thresholds, which represent the quality of the fit (i.e. 1 corresponds to a perfect fit, whereas 0 to a poor fit). Therefore, simulations which result in an R^2 value below a specific threshold are eliminated.

In a second step, simulations which are subject to a small relative volume change are removed. This is important as these data have a strong tendency of yielding unreasonably long e-folding times.

In the third and last filtering step, the equilibrium state at the very end of a simulation is examined, by analyzing the respective volume change. Glaciers which do not reach a steady state are removed. This is done by examining the last years of the time series and removing simulations, which are subject to volume changes above a certain threshold.

Filtering process stabilization time

In contrast to the e-folding time, data which is used to obtain the stabilization time do not have to follow an exponential fit. Hence, this filtering process directly starts by excluding data which only simulate a small relative volume change. The reasoning behind this filter is the same as for the e-folding time, to exclude unrealistically long stabilization times for a small volume change.

In the second and last step, the steady state filtering is applied. Again, this procedure is applied to ensure that only simulations which have reached a steady state are included.

3.4 Obtaining the response time

Comparing different volume response times (hereafter typically referred to as response time) with each other is not straight forward. This is primarily because they are strongly influenced by the temperature forcing applied: For instance, in scenarios with a strong warming, glaciers will experience a much more rapid loss of ice mass compared to cases with a weak warming. Consequently, this leads to a faster response time for glaciers in the former case. Hence, assigning a single value to characterize a region becomes difficult, as it depends on the simulated climate scenario. Therefore, a method which simplifies comparison is applied to the process by plotting all e-folding and stabilization times within a region with respect to their relative volume changes. Thus, by characterizing the response time with an underlying volume change, different e-folding and stabilization times are normalized to enable a comparison with each other.

3.5 Random forest setup for response time prediction

As part of this thesis' analysis, a random forest is trained on various glacier features like slope or ice thickness, in order to predict the response time of different regions. This algorithm further allows for the analysis of important factors that influence the response time of glaciers, by analyzing the structure of the decision tree. In the following, a brief introduction on the advantages of using such algorithm is provided.

The random forest algorithm, first introduced by Breiman (2001), consists of multiple randomized decision trees. In order to be able to predict the response time of a region, a regression random forest is used, since the goal is to predict a specific numerical time. In this case, every decision tree yields one prediction, which is then averaged over all trees, resulting in an overall prediction (Biau & Scornet, 2016). This averaged prediction corresponds to the predicted response time.

Using a random forest for prediction has the advantage of being able to examine the automatically generated decision trees (Biau & Scornet, 2016), hence, it does not represent a "black box" compared to other machine learning models. Therefore, by analyzing the tree structure, important information about the driving parameters for the response time can be derived. These driving parameters are represented by the algorithm's features, on which the random forest is trained on. It is important to note, that the correlation between these features should be small in order for the random forest to be stable (Nan et al., 2015; Strobl et al., 2008). For instance, using both the area and volume of a region will negatively impact the algorithm's prediction quality as these two parameters are strongly related to each other. In this thesis, different combinations of features are investigated, described in Section 4.4.

4 Results

The results of the applied filtering process for obtaining the response time are examined in Section 4.1 and 4.2. The resulting regional e-folding times are described in Section 4.3. Finally, section 4.4 shows the prediction quality of the trained random forest and gives insights into the underlying features.

4.1 Filtering

4.1.1 Filtering e-folding time

As described in Section 3.3.2, the filtering process is divided into three steps. First, simulations which do not follow an exponential fit are removed. This is done by eliminating data below a certain R^2 threshold. After testing numerous thresholds empirically, we found that an R^2 value of 0.95 is reasonable. An overview of this filtering process is shown in Fig. 9. The simulation represented by the orange line yields an R^2 value which is smaller than the threshold and, thus, is removed.
In the second step, simulations which are subject to small relative volume changes are eliminated. These simulations are represented in Fig. 9 by gray lines. As can be seen, their R^2 value is greater than 0.95 and, thus, are not being removed by the exponential fit filtering. By plotting the unfiltered calculated e-folding time with respect to its volume change in Fig. 10, the importance of this additional filtering step becomes apparent. The color of each e-folding time corresponds to the R^2 value. The figure shows that the R^2 threshold filtering (i.e. the first step) leads to the exclusion of small volume change simulations in the left plot and, thereby, eliminating e-folding time which result in extremely large values. Contrary, the e-folding times in the right part of the figure show, that these extremely slow response times for little volume changes are not removed by the R^2 threshold filtering. Therefore, the relative volume filtering has to be applied in order to remove unrealistically long response times for such small volume changes.
The third and last filtering step consists of removing simulations, which have not reached a steady state by the end of the time frame. This is done by examining the last 10% of the time series and removing data, which have a volume change larger than 5% throughout this time. An example is shown in Fig. 9, where the green line clearly shows that no steady state has been reached. In this figure, the threshold is set at a maximum relative volume change of 5% during the last 500 years (which corresponds to the last 10% of the time series). Note that this green line is exaggerated in order to facilitate the visual comparison. The other lines correspond to real simulations.
After applying the three described filtering steps, only data corresponding to blue lines in Fig. 9 are used for determining the e-folding time (only two are shown for visualization purposes).

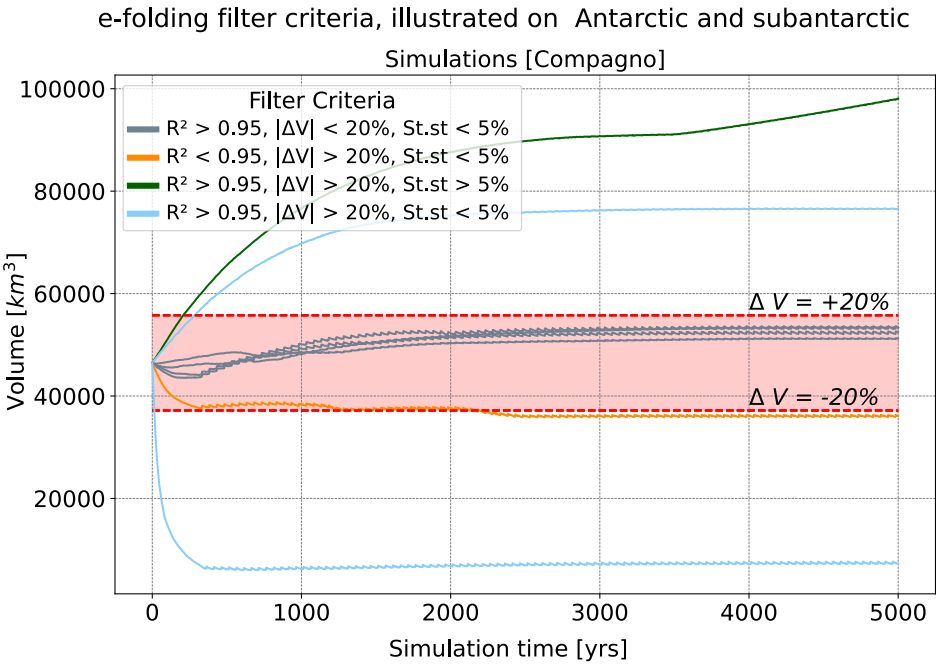

Figure 9: Applied filtering process for obtaining e-folding time. Only data corresponding to the blue lines are considered. R^2 shows the exponential fit (1 represents a perfect fit whereas 0 a poor fit). R^2 threshold is set to 0.95. $|\Delta V|$ corresponds to the absolute relative volume change. A minimum relative volume change of $|\Delta V| = 20\%$ is selected. St.st represents the maximum relative volume change during the steady state i.e. in the last 10% of the time series (here, this would correspond to the last 500 years). The steady state threshold is set to 5%. Note that the green line is exaggerated to facilitate the visualization while the others represent true simulations.

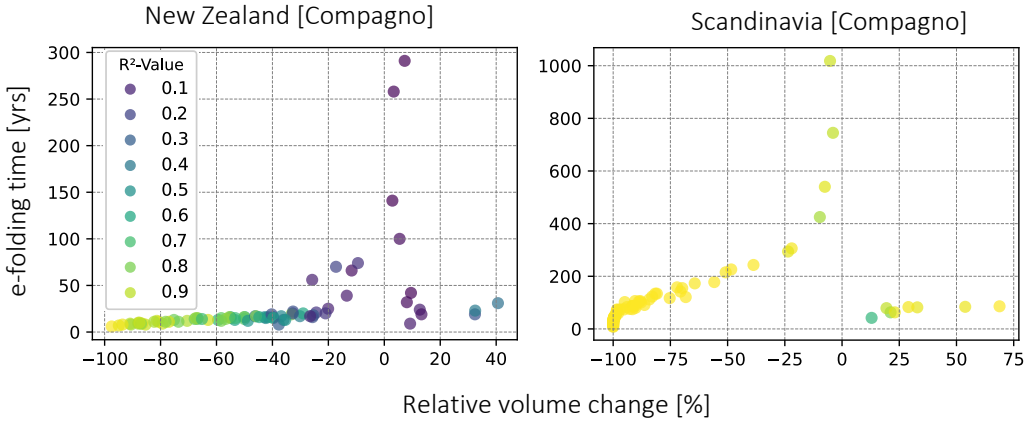

Figure 10: e-folding time with respect to the relative volume change. Color scale shows the exponential fit (i.e. R^2 value). **Left:** e-folding time for New Zealand shows an extreme peak around 0% relative volume change. Due to their poor exponential fit they are removed by the exponential threshold filtering. **Right:** Simulations for Scandinavia also show an unrealistic peak around 0% relative volume change. Due to their good exponential fit, they have to be removed with an additional filtering method, i.e. by removing data within a very small relative volume change.

4.1.2 Filtering stabilization time

In contrast to the e-folding time, data which are used to obtain the stabilization time do not have to follow an exponential fit. Hence, this filtering process directly starts by eliminating simulations with an absolute volume change, which is smaller than 20%, as depicted in Fig. 11. In a second step, data that have not reached a steady state during the last 10% of the time series are removed. By setting a maximum relative volume change of 5% during this time frame, the same procedure as applied for the e-folding time is conducted. The remaining data which are used for obtaining the stabilization time are shown as blue lines in Fig. 11. By comparing Fig. 9 with Fig. 11, it becomes clear that the e-folding process removes more simulations compared to the stabilization one.

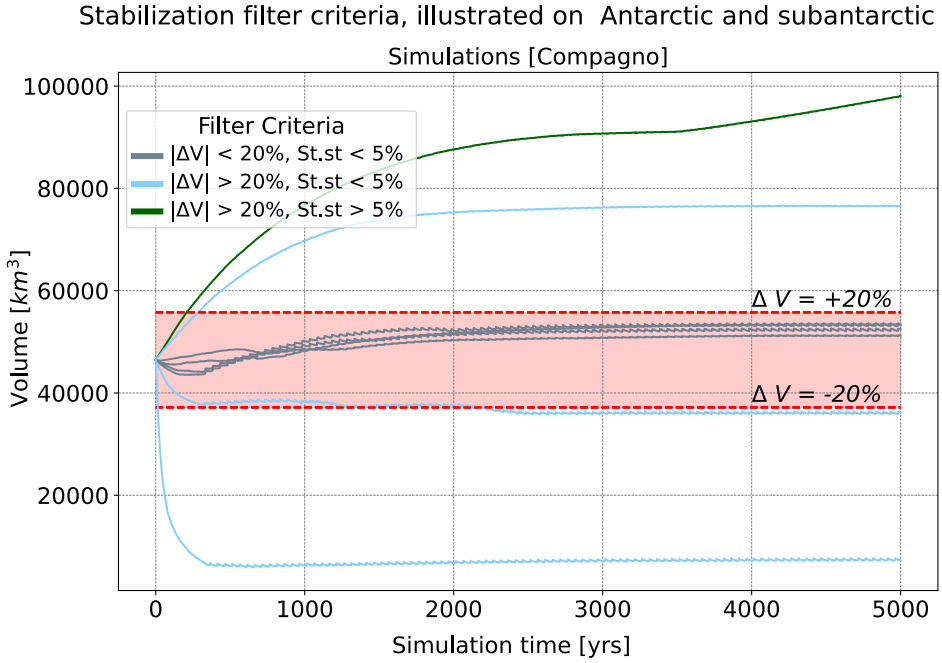

Figure 11: Applied filtering process for obtaining stabilization time. Only data corresponding to the blue lines are used for obtaining the stabilization time. $|\Delta V|$ corresponds to the absolute relative volume change. A minimum relative volume change of $|\Delta V| = 20\%$ is selected. St.st represents the maximum relative volume change during the steady state in the last 10% of the time series (here, this would correspond to the last 500 years). The steady state threshold is set to 5%. Note that the green line is exaggerated to facilitate the visualization while the others represent true simulation data.

4.2 Functional fit through obtained response times

After filtering, the remaining simulations are used to obtain the e-folding time. Note that this process is identical to the one for the stabilization time. The results of the latter are analyzed in further detail in Section 5.4.

The regional e-folding time can be obtained by plotting the obtained times for all climate scenarios within a region with respect to their relative volume changes (i.e the same procedure as

in Fig. 10, but after applied filtering). The left plot in Fig. 12 shows such an example for Central Asia. As can be seen by the color coding, the models Rounce, Compagno, Kraaijenbrink, GLIMB, OGGM_v1.6 and OGGM-VAS simulated this specific region. Another example is given for Western Canada and United States in Fig. 13.

Due to the fact that many models were not run for an increase in mass balance scenario (i.e. in a case where the glaciers gain volume), the e-folding time analysis is limited to a glacier mass loss scenario only. This is the reason why the x-axis in Fig. 12 and 13 include negative volume changes only.

The obtained model points are then fitted with a 3^{rd} order polynomial function, resulting in the right plot of Fig. 12 and 13. Hence, each line reflects a model's e-folding time function, which is dependent on the relative volume change. A 3^{rd} order polynomial fit is selected over a linear fit due to the already strong similarity of the obtained data points in the left part of both figures to such a fit. However, a comparison to a linear fit is briefly shown in Section 4.3 as well.

In order to now obtain the e-folding time for each region, three different relative volume loss scenarios are defined, where the corresponding e-folding times per model are selected. These selected times represent the regional e-folding time per model for a volume loss scenario at 75%, 50% and 25%.

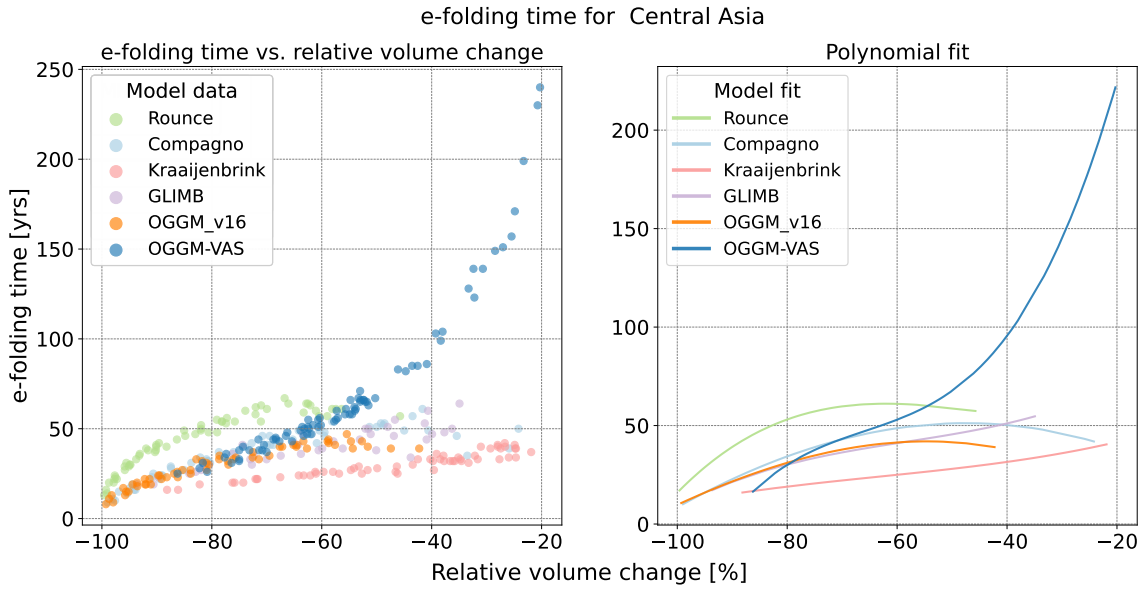

Figure 12: Example for Central Asia. **Left:** Plot shows e-folding time with respect to the relative volume change. All models which performed glacier simulations for Central Asia are included. **Right:** 3^{rd} order polynomial fit through the data points from the left graph.

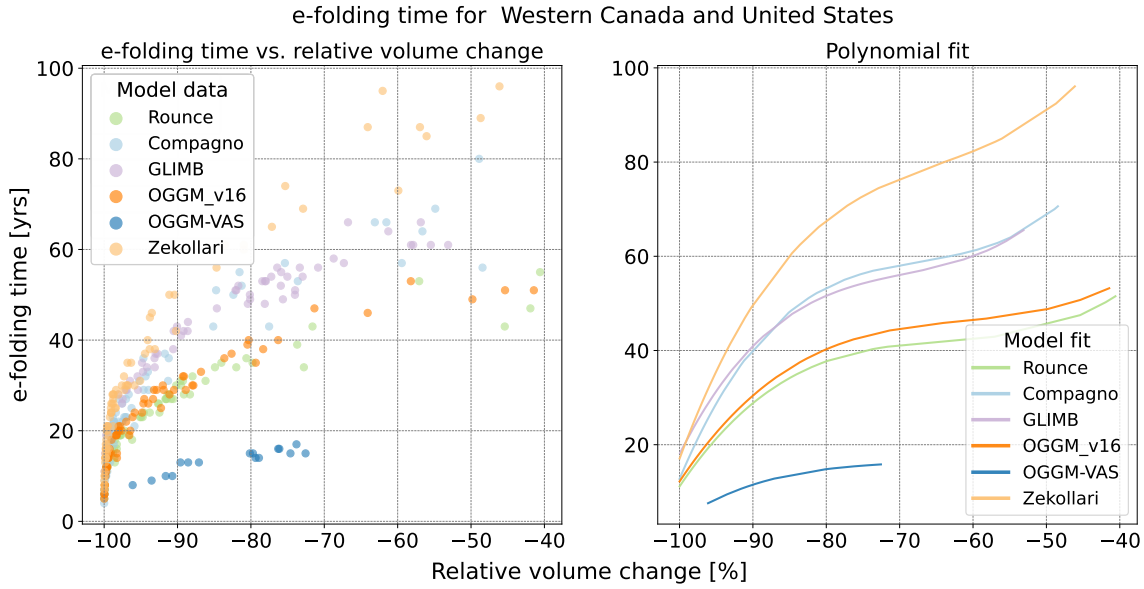

Figure 13: Example for Western Canada and United States. **Left:** Plot shows e-folding time with respect to the relative volume change. All models which performed glacier simulations for this specific region are included. **Right:** 3^{rd} order polynomial fit through the data points from the left graph.

4.3 e-folding time

The e-folding time for all 19 regions is displayed in Fig. 14. The plot distinguishes between three different volume losses, i.e. it shows the regional e-folding time for a loss of 75%, 50% and 25%. The different colors correspond to the various models which simulated glacier retreat under different climate scenarios. The blue bars represent the mean ice thickness which is obtained by dividing the total volume of a region by its area. Since the volume of a region is somewhat arbitrary (see Fig. 7), Fig. 14 is sorted by its mean ice thickness instead as it represents a better parameter to compare the different regions with each other. The process of obtaining this e-folding overview figure, which is described in the previous sections, is summarized in an overview flowchart in the appendix in Fig. A.1.

In Fig. 14 it is visible, that not every region includes the same amount of models (e.g. region Arctic Canada North at a 75% volume loss shows four models whereas region Russian Arctic includes five). The same applies to the three different simulated volume losses (e.g. region Arctic Canada South includes five simulations for a volume loss of 75% but only shows one simulation for a 25% loss). This is because not all models performed simulations on all 19 regions. Further reductions arise due to some models not simulating all three volume loss scenarios as well as due to the fact that certain simulations were eliminated during the filtering process.

The regional e-folding overview plot (Fig. 14) shows, that the obtained response time can vary strongly between different models: GLIMB predicts the Russian Arctic to take roughly 700 years to reach its e-folding time in the case, where half of the region's volume is lost.

Simulations with OGGM-VAS, on the other hand yield an e-folding time of 190 years for the same volume loss. While this spread between the models is small for regions with a small mean ice thickness, it is substantial for areas with thicker masses of ice.
In order to facilitate the comparison between regions, the mean regional e-folding time obtained through the results in Fig. 14 is displayed in Fig. 15. The black points represent the mean response time while the small gray points correspond to the e-folding time from the different models. As in the previous figure, the mean regional e-folding time is sorted by increasing mean ice thickness. Since some regions only include one result from one model, the mean e-folding time for those specific regions corresponds to the e-folding time of a specific model. For instance, in Arctic Canada South at a 25% loss, the e-folding time obtained from OGGM-VAS corresponds to the mean e-folding time.
By comparing the different mean e-folding times between regions, it can be seen that for most regions with a small mean ice thickness, the time to adjust to a new warming climate steady state is fast. On the contrary, with increasing ice thickness, the e-folding time seems to become longer. This behaviour is visible in all three subplots, i.e. throughout all three different simulated volume losses. There are, however, some exceptions. By looking at the Southern Andes and Alaska, it becomes apparent, that despite of the two regions' large mean ice thicknesses, both adjust to warming climate scenarios extremely fast. The mean e-folding time is almost the same as Central Asia or Central Europe, which in contrast have a roughly 70% smaller mean ice thickness. This fast e-folding time does not come from a bias due to only one model being available in those regions. The mean e-folding time for both regions was obtained from at least four models in each volume loss scenario.
Another characteristic, which is visible in Fig. 15, is the dependence on the simulated volume loss. A region responding to a large volume loss generally corresponds to a faster response time. While for some regions, this behaviour is very small, other regions show a significant increase: The Arctic Canada South e-folding time increases by almost 400 years between the 25% and 75% volume loss.
This mean e-folding time in Fig. 15 is, as addressed in previous figures, obtained by fitting a 3^{rd} order polynomial fit through the data points. The selection of such a polynomial fit over a linear fit does, however, not yield a strong difference, as can be seen in Fig. A.2. The linear fit version yields almost the exact same mean regional e-folding time with Russian Arctic showing a slightly faster response time in case of a 75% volume loss.

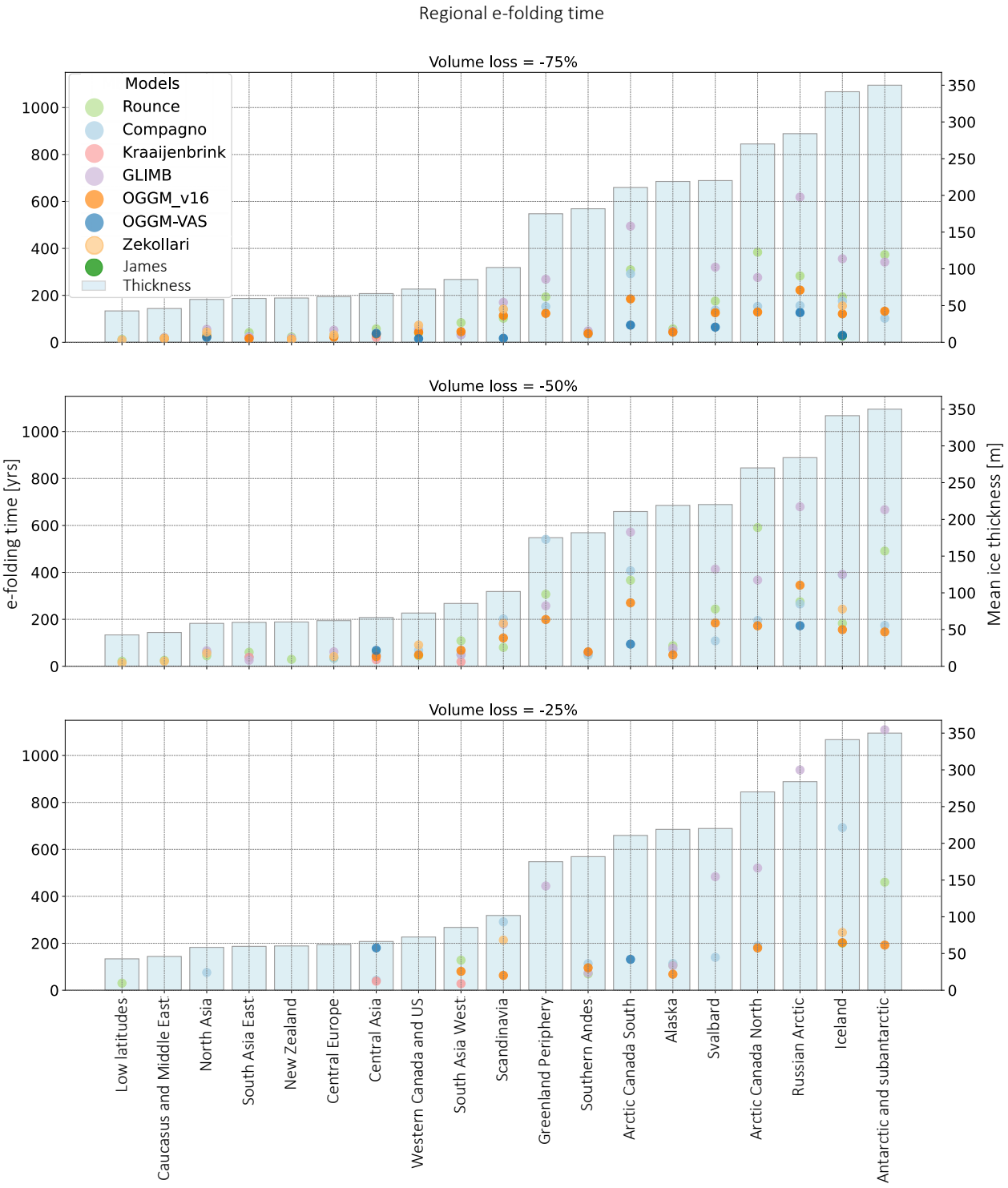

Figure 14: Regional e-folding time obtained for three different volume-loss scenarios, i.e. at a 75%, 50% and 25% loss. Colors correspond to the different models used for simulation. The regions are sorted by the mean ice thickness, represented by the blue bars. Y-axis limit is set to be the same for all three subplots in order to facilitate comparison.

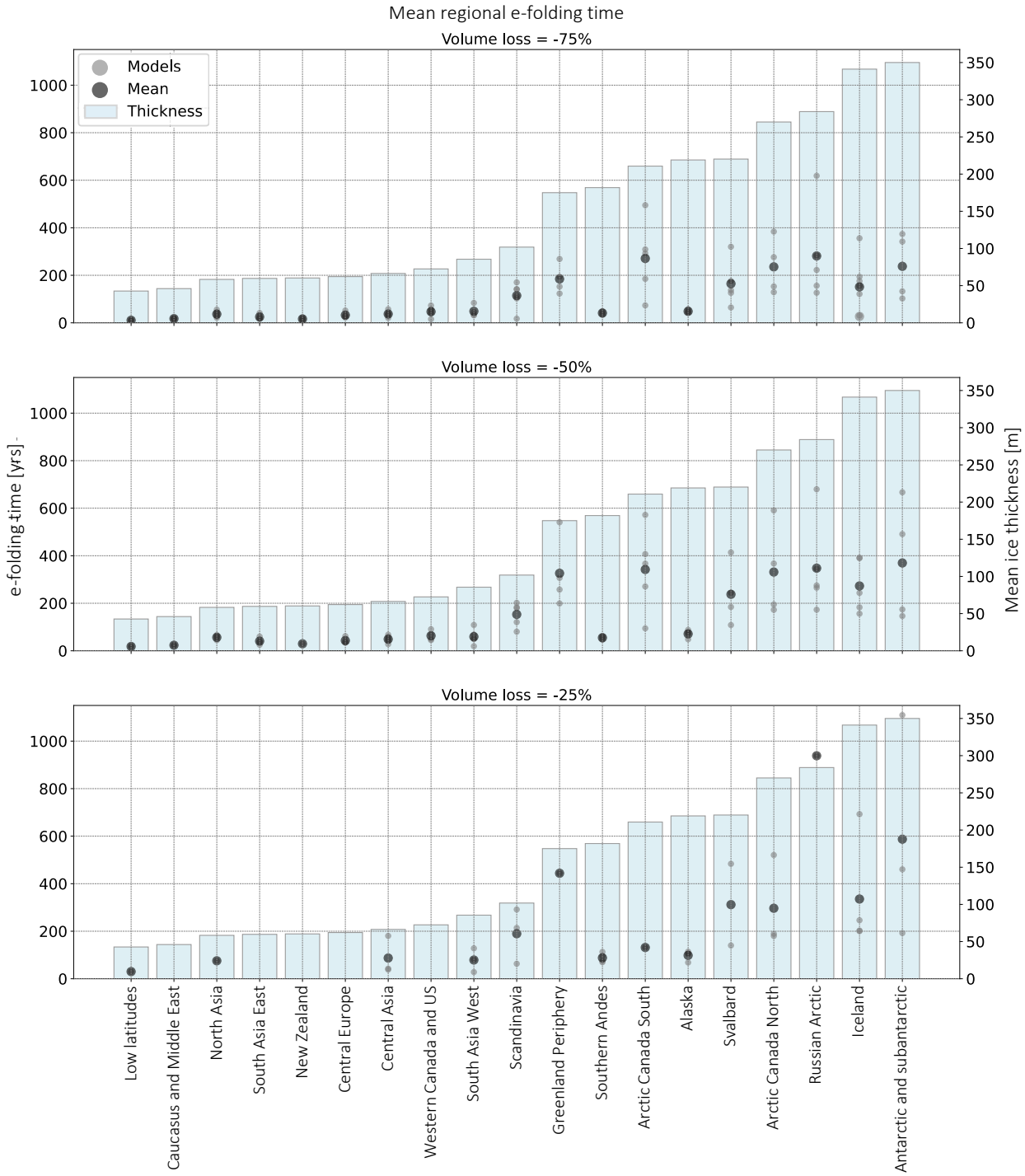

Figure 15: Mean regional e-folding time obtained for three different volume-loss scenarios, i.e. at a 75%, 50% and 25% loss. Grey dots represent the individual e-folding times per model. Black dots display mean regional e-folding time, obtained by calculating the mean between the different model-results per region. The regions are sorted by the mean ice thickness, represented by the blue bars. Y-axis limit is set to be the same for all three subplots in order to facilitate comparison.

4.4 Random forest

The random forest algorithm in this thesis is mostly used as additional help to asses differences in regional e-folding times as well as deviations between models by investigating the decision tree structure. Therefore, the focus of this section is on the set up of the algorithm, rather than the actual predicted e-folding time.

The prediction algorithm used in this thesis is a 5-fold random forest. This means that the complete underlying training dataset is split into five sub-sample groups. This process enables a prediction for each obtained e-folding time. Otherwise, if the algorithm was trained on 70% of the data, only 30% could be used for testing and comparing.

The random forest in this thesis is trained on the features described in Table 5. It is worth mentioning that using the area or volume is not an indicative feature for a specific region. This is due to the fact that these regions are somewhat randomly defined (see Fig. 7). To still include a measure of glacier size, the mean ice thickness is used, which is derived from the area and volume of the region. Additionally, the simulated volume change as well as the mean slope of a region are used as features. The latter is derived by taking the mean slope of all individual glaciers and weighting them by their size. Not only does this parameter reflect a region's slope, but it is also indicative whether an area corresponds to an ice-cap or a mountain glacier dominated region. In regions with small mean slopes, large ice caps are typically present whereas a steep slopes are associated with mountain glacier-dominated areas. Further features on which the algorithm is trained on are represented by a calving and a polar index. While the former determines whether calving occurs in regions, the latter ranks them by their latitude.

Table 5: Features which are used to train the random forest algorithm.

Features	**Description**	**Values used**
Mean thickness	The mean regional ice thickness, which is derived by dividing the regional volume by its corresponding area, is used.	Effective mean ice thickness in m
Volume change	The algorithm receives the respective relative volume change for each simulation.	-75%, -50%, -25%
Mean slope	This feature corresponds to the mean slope of all individual glaciers within this region, weighted by their size. A steep mean slope indicates a mountain glacier dominated region whereas a gentle slope is indicative for an ice-cap dominated one.	Effective slope in %
Calving	Whether calving occurs.	0 (Not calving), 1 (Calving)
Polar index	A polar index has been established which classifies regions into *not polar*, *mid-latitude*, *mildly polar* and *polar*.	0 (not polar), 1 (mid-latitude), 2 (mildly polar), 3 (polar)

The random forest e-folding time predictions are displayed in Fig. 16. The x-axis represents the true e-folding time from the previous section (Fig. 14). The y-axis corresponds to the predicted values. Hence, if the algorithm perfectly predicts the e-folding time, a point shows up on the blue dashed line. A data point above the blue line indicates that the algorithm overestimated the e-folding time whereas underestimated predictions are located below the blue line. The mean relative error corresponds to 39.4% while the maximum relative error is equal to 114.6%. It can be seen, that with increasing e-folding time, the prediction becomes less accurate. In other words, the scattering in Fig. 16 increases by moving to the right. Furthermore, there is a tendency of underestimation for long response times while overestimation seems to be present for fast to intermediate e-folding time predictions. Additionally, it seems that the model performs poorly on GLIMB predictions. In order to compare the predictions between regions as well as between different volume loss scenarios, an overview graph is visible in Fig. A.3. As seen in previous figures, the color coding corresponds to the different models used for simulations and the graph is sorted by increasing regional ice thickness. Additionally, filled circles correspond to the obtained e-folding time from Fig. 14. Outlined circles indicate the predicted values by the random forest. For each volume loss scenario, the mean relative error as well as the mean relative maximum error is shown. The figure shows that predictions in which regions lose half of their volume, lead to the smallest relative mean error of 29%.

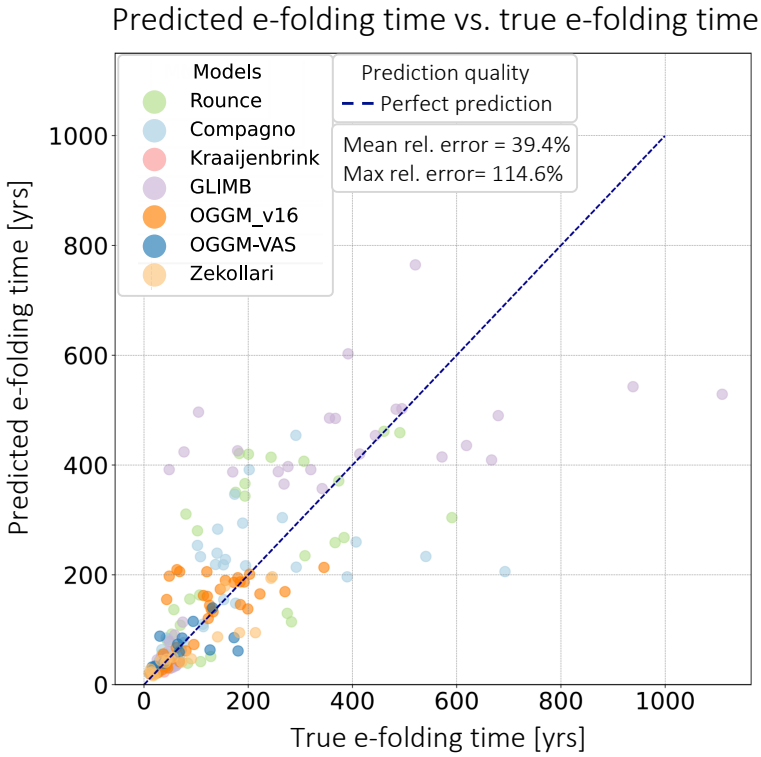

Figure 16: e-folding time predicted with a random forest algorithm. X-axis corresponds to the true e-folding time, i.e. the obtained values from Fig. 14. Y-axis represents e-folding time predicted by the algorithm. Colors correspond to the different models. Blue line shows location where the predicted time is equal to the true one.

5 Discussion

This thesis' discussion is divided into four sections. Section 5.1 investigates the key drivers of the e-folding time by examining the structure of the random forest. Furthermore, the regions are ranked by their e-folding time, providing insights on fast and slow regions on Earth. Section 5.2 explores differences between the models used in this thesis, categorizing them into slow, intermediate and fast models. The limitations of the trained random forest are discussed in Section 5.3 and Section 5.4 delves into the discussion of using a stabilization time instead of the well established e-folding time.

5.1 Regional comparison

5.1.1 Random forest assessment

As previously mentioned, the random forest algorithm trained in this thesis is primarily used to understand the driving forces behind the regional e-folding time. It has become apparent that the different e-folding times between regions in Fig. 15 cannot only be explained due to the mean ice thickness (see Alaska and Arctic Canada, where both have a similar ice thickness but very different response times), although there seems to be a tendency of longer e-folding times with larger ice thicknesses.
The generated decision trees in a random forest can become very large and chaotic. An example of such a tree is shown in Fig. A.4. The depth in this specific tree, which was created for predicting the e-folding time of the Rounce model, has been limited to three nodes only for visualization purposes. This, however, does not reflect the reality of these trees. Without limiting this specific tree's depth, it would have had a depth of seven to eight nodes. An assessment of these trees is therefore, due to their sheer complexity, challenging.
However, since the decision tree tries to incorporate the most relevant feature within a training dataset as root node, i.e. the uppermost element, the overall parameter importance can be examined. Fig. 17 shows a summary of these features. The parameters are ranked by their occurrence as root (upper part in the figure) or child feature (lower part). Additionally, the threshold on which the algorithm decides whether to move to the right or left in a tree (see example sketch on the left) is provided for the root level. As shown, the ranking indicates that the regional mean slope is the most important parameter which has the strongest influence on the region's e-folding time, followed by the mean ice thickness. The volume loss seems to be somewhat important, whereas the ranking of the polar index and calving suggest only minor influence. However, this ranking needs to be interpreted with caution since various features show some correlation, as shown in Fig. A.5 (e.g. mean slope and polar index, mean slope and mean ice thickness). This indicates that the polar index is potentially more relevant than ranked here. Nevertheless, the most important parameter remains the mean slope, followed by the mean ice thickness, which is explained more closely in Section 5.1.2.

To analyze the results obtained from the random forest, the mean e-folding time with respect to the region's slope is shown in Fig. 18. Additionally, the weighted mean threshold of 13.1% obtained from the table in Fig. 17 is represented by a blue dotted line. By examining the threshold, it becomes clear that it acts perfectly as a divider between slow response times and fast ones for large and medium volume losses. In case of a loss of 25%, however, the divider does not seem to have the same effect, as there are some fast e-folding times at a slope of around 12% as well. Obtained e-folding times for such little volume losses do, however, have to be carefully interpreted. This is due to the fact that there are less models available, which simulated such small volume losses (see Fig. 14 for comparison). Hence, for such cases, the mean e-folding time can be the result of just one model. Therefore, the 13% slope threshold seems to represent a good approximation to distinguish between fast and slow regions. An additional behaviour which can be seen in the same figure is the independence between slope and e-folding time above and below the threshold. For steeper regions (i.e. above 13%), the response time is almost independent of the slope. Only areas with a slope greater than 24% seem to be further affected by the steepness, resulting in a faster e-folding time. For regions below 13%, it is not as clearly defined due to the points being more scattered. Though there might be a tendency of following a constant response time between 5% and 13% (irrespective of the slope).

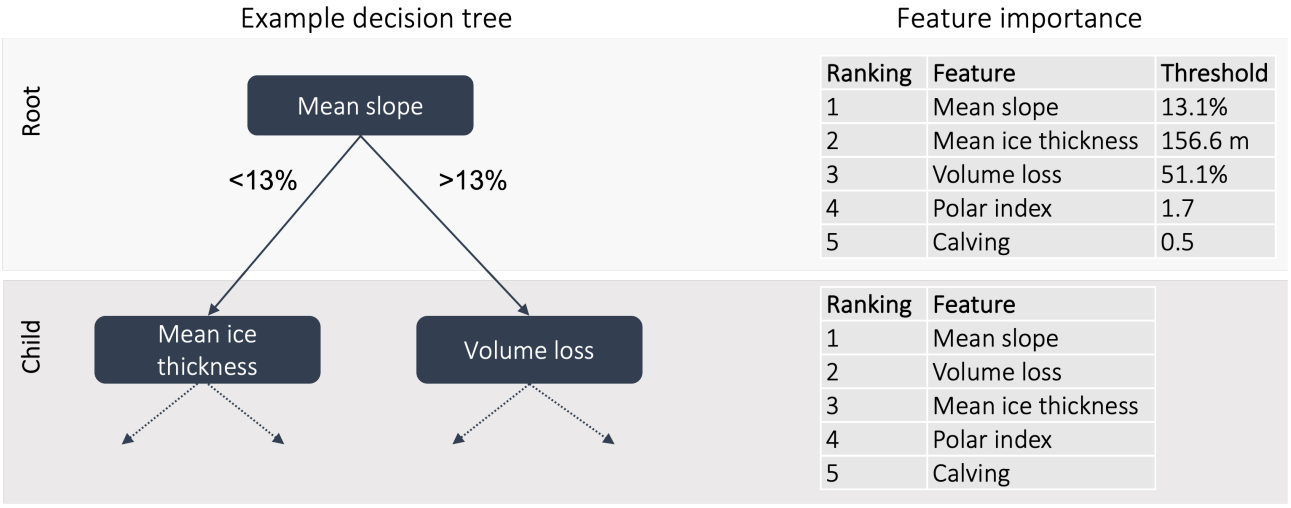

Figure 17: Left part shows example decision tree with the first two elements, i.e. the root and child node. Accordingly, the features are ranked by their occurrences as root or child node throughout all models and regions in the right table. For the root features, the weighted mean threshold values are displayed.

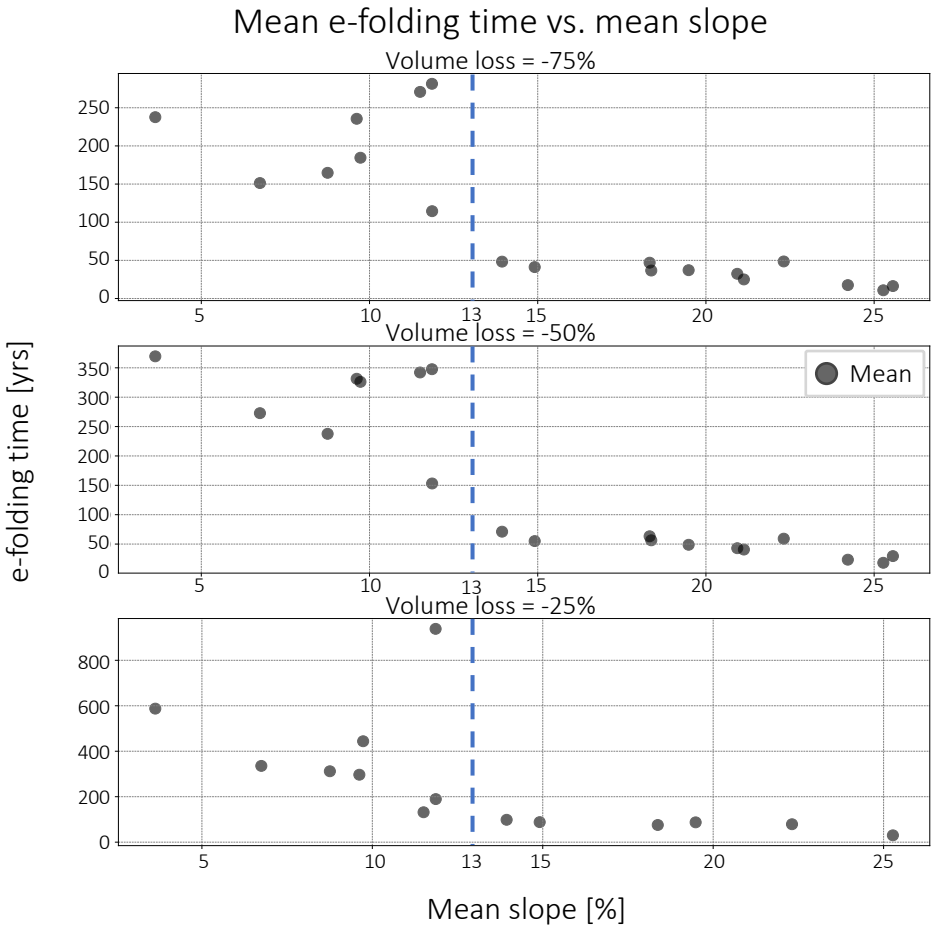

Figure 18: Mean e-folding time plotted with respect to the region's mean slope. Blue line shows location at 13%, which corresponds to the threshold determined by the random forest. In case of medium to small volume losses, the threshold almost perfectly divides the regions into fast adapting and slow adjusting ones. Note that the y-scales are different for all volume loss scenarios.

5.1.2 Qualitative assessment and ranking

As described in the previous section, the random forest examination revealed that the slope is the most important feature for the regional e-folding time. This aligns well with the study by Zekollari et al. (2020), where they investigated the response time of the European Alps. The group found that the response time of the European Alps is primarily driven by the glacier slope. This relationship is further displayed on Fig. 19, where the regional e-folding time is sorted by increasing slopes (blue bars). It is visible that almost all regions which correspond to a mean slope below 13% lead to slow e-folding times which are well above 100 years. Only Scandinavia, in case of 75% volume loss, shows signs of a slightly faster response time of 114 years. By distinguishing between regions above and below the slope threshold and examining the region's dominated glacier type, two key findings are revealed. Regions, which are dominated by a small mean slope and in which large ice caps are typically present yield

a slow e-folding time and mountain glacier dominated areas, which are represented by steep slopes, result in a fast e-folding time. Additionally, by comparing this Fig. 19 with the RGI-overview one (Fig. 7), it becomes apparent that regions belonging to high latitudes take longer to adjust (e.g. Antarctic and subantarctic, Iceland, Svalbard, Arctic Canada North etc.). In contrast, low latitude regions (e.g. New Zealand, Caucasus and Middle East, South Asia West etc.) are related to fast response times. This contradicts the feature ranking in Fig. 17, where the polar index seems to be less important, but confirms the correlation between the features mean slope and polar index shown in Fig. A.5. This particular correlation might affect the random forest algorithm to result in the assumption of the polar index being less significant, which, as described, is not the case. However, the algorithm's ranking of the features mean slope and mean thickness are verified by examining Fig. 15 and Fig. 19, where the latter clearly shows that the mean slope has a stronger influence on the response time than the mean ice thickness. For instance, Alaska and Southern Andes represent outliers in the plot sorted by mean ice thickness (Fig. 15) due to their fast response time despite having a large mean thickness (e.g. in a 75% volume loss scenario). If the regions are sorted by increasing slope (Fig. 19), however, both regions fit in well with their fast response time due to their steep slopes. Additionally, the polar index might not be a very relatable representation since the regions are somewhat arbitrarily defined. Thus, while this random forest algorithm is affected by feature correlation, the ranking of the two most important parameters (i.e. mean slope followed by mean ice thickness) are not.

To identify and rank fast and slow responding regions, an overview including all RGI regions is presented in Table 6 . This table shows the regional mean e-folding time with its associated uncertainty for the 75% and 50% volume loss scenario. The third loss scenario is excluded as some regions do not include a mean e-folding time (e.g. South Asia East). Additionally, the general model availability for each region is scarcer in case of a 25% loss, leading to greater uncertainty. The regions in the two different volume loss scenarios in Table 6 are sorted by increasing e-folding time. Furthermore, the number of available models are added. As shown, the e-folding time for the 75% volume loss ranges between 10.8 $\pm$ 1.0 and 281.4 $\pm$ 88.5 years. This is slightly faster compared to the case of a 50% loss, where the response time lies between 18.1 $\pm$ 3.4 and 369.6 $\pm$ 126.2 years. Having a region adapting to a large volume loss faster than to a small one might first seem counterintuitive. This is, however, likely the result of the applied climate forcing: In case of strong warming, the glacier will lose mass very rapidly. If only a weak warming scenario is applied, the glacier's size decreases much more slowly. Despite these differences between large and medium volume changes, the overall ranking between the two scenarios remains very similar. This can be seen by comparing the four fastest regions for both volume losses with each other. Except for New Zealand, the ranking is the same for both scenarios. The slight difference might be the result of only having one available model for the 50% loss scenario. This observation indicates that the ranking of regions is independent of the amount of volume loss they experience.

The difference in model availability in Table 6 might introduce some bias as some models have a tendency of producing faster or slower response times. For instance, if a region includes two models only, and one of them is known to yield a very fast e-folding time, the mean response time of this region will be strongly affected. Hence, the aforementioned case will likely result in an underestimation of the region's response time. To counter this effect, a second e-folding ranking is shown in Table A.1, for which only four models with an almost global coverage are used (GLIMB, Rounce, Compagno and OGGM). Note that in two regions, only three out of the four models were available.
Thus, the bias resulting from the different amount of models used to obtain the response time is reduced. The ranking is only displayed for a 75% volume loss due to limited model availability. By comparing Table A.1 with Table 6, it can be seen that there are only minor differences between the ranking (e.g. Russian Arctic and Arctic Canada South are switched). However, the new approach shows a tendency of resulting in slower response times (e.g. Arctic Canada South predicts an e-folding time of 270.8 $\pm$ 70.1 years in Table 6 while Table A.1 projects a 320.2 $\pm$ 64.4 years response time. This difference between model predictions is the result of some models exhibiting slower e-folding times and is explained in the next section 5.2. Hence, while the use of different number of models for ranking may introduce some bias, it does not have a significant impact on the overall regional ranking presented in Table 6.

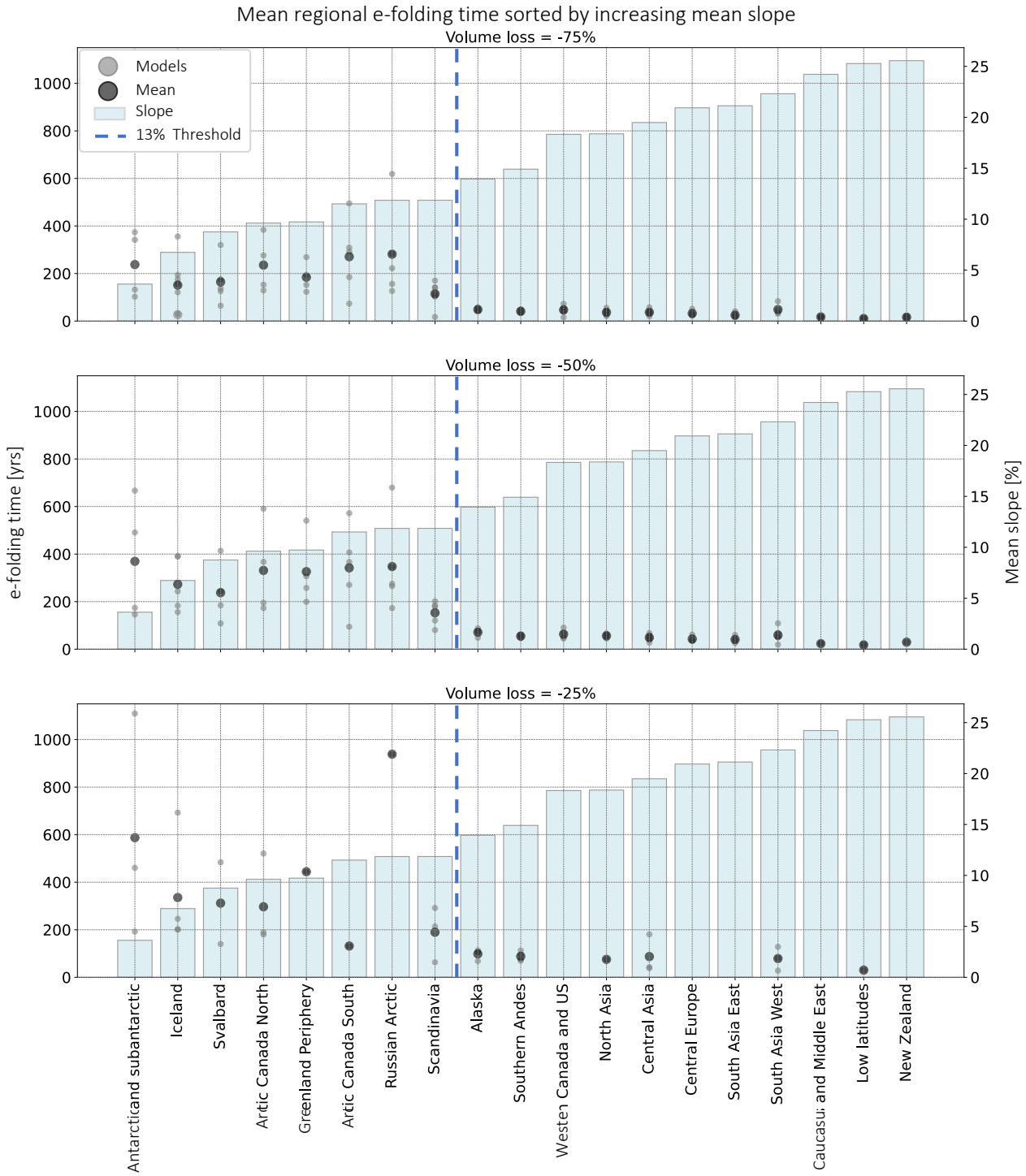

Figure 19: Mean regional e-folding time sorted by increasing mean slopes (blue bars). Gray dots represent e-folding times from the different models. Blue dashed line represents the 13% mean slope threshold obtained with the random forest from Fig. 17.

Table 6: Mean regional e-folding time for a 75% and 50% volume loss scenario. Regions are sorted by increasing e-folding time. For each area, the number of models from which the e-folding time is calculated is displayed. The uncertainty is obtained by dividing the standard deviation of the samples for each region by the square root of the number of samples. Since there is only one model for New Zealand in a 50% volume loss scenario, no uncertainty is provided in this specific case.

75% volume loss scenario		
Region	e-folding time [yrs]	# Models
Low latitudes	10.8 ± 1.0	3
New Zealand	16.3 ± 2.4	4
Caucasus and Middle East	17.6 ± 0.9	5
South Asia East	25.0 ± 4.4	5
Central Europe	32.4 ± 5.1	5
North Asia	36.7 ± 5.1	6
Central Asia	37.1 ± 4.8	6
Southern Andes	41.2 ± 3.3	4
Western Canada and US	47 ± 7.8	6
Alaska	48.3 ± 3.1	4
South Asia West	48.6 ± 12.1	4
Scandinavia	114.5 ± 21.6	6
Iceland	151.3 ± 42.3	7
Svalbard	164.7 ± 42.7	5
Greenland Periphery	184.5 ± 31.5	4
Arctic Canada North	235.5 ± 59.0	4
Antarctic and subantarctic	237.7 ± 69.9	4
Arctic Canada South	270.8 ± 70.1	5
Russian Arctic	281.4 ± 88.5	5

50% volume loss scenario		
Region	e-folding time [yrs]	# Models
Low latitudes	18.1 ± 3.4	2
Caucasus and Middle East	23.4 ± 1.9	2
New Zealand	29.5 ± x	1
South Asia East	40.6 ± 7.1	4
Central Europe	43 ± 6.4	4
Central Asia	48.8 ± 5.6	6
Southern Andes	55.1 ± 3.3	4
North Asia	56.4 ± 4.5	4
South Asia West	59.2 ± 14.6	5
Western Canada and US	63.3 ± 10.5	4
Alaska	71.0 ± 8.28	4
Scandinavia	153.1 ± 22.7	5
Svalbard	237.6 ± 64.9	4
Iceland	272.8 ± 50.1	5
Greenland Periphery	326.1 ± 74.8	4
Arctic Canada North	331.3 ± 96.8	4
Arctic Canada South	342.1 ± 78.7	5
Russian Arctic	347.6 ± 87.4	5
Antarctic and subantarctic	369.6 ± 126.2	4

5.2 Model comparison

For many years, the difference between the models' predicted volume loss was difficult to explain. These difficulties emerged because the models were limited to simulating glacier mass loss until the end of the century. As glaciers are not expected to reach a steady state by 2100, drawing definitive conclusions about the behaviour of these simulations became challenging. With the GlacierMIP3 experiments, simulations were performed over a prolonged time frame, allowing for glaciers to reach equilibrium. Due to these steady states, GlacierMIP3 experiments provide valuable insights into the response times of regions, allowing for a better understanding of model behaviour. For instance, if a model has a tendency of yielding a slower response time compared to others, the predicted volume loss by 2100 should be interpreted with caution as the simulated volume loss is projected over a longer time scale. Therefore, the predicted volume loss by 2100 might be underestimated. Hence, knowing which models lead to conservative predictions and vice versa is key for interpreting current and future glacier loss predictions.

5.2.1 Qualitative assessment

Assessing the difference in e-folding time between models is partially done in a qualitative way by examining Fig. 20. An additional quantitative model ranking system was tested as well (not shown in this thesis), though its applicability remains very limited due to the fact that not all models simulated all RGI regions.
The Fig. 20 shows the regional e-folding time for all models with respect to the slope and mean ice thickness. Note that the y-axis varies between the different volume loss scenarios. A ranking and summary of key findings, starting from the slowest model, is provided in Table 7. By examining Fig. 20, it becomes apparent that simulations by GLIMB yield very slow response times. This comes as a surprise as the model uses a volume-area approach, which is considered to result in fast response times due to ice-flow dynamics being neglected. In contrast, simulations from OGGM-VAS, which is also a volume-area scaling model, shows very fast response times as expected. Although the models are similare, there are two distinct differences. While GLIMB's mass balance is based on an energy balance model, OGGM-VAS uses the degree day method. Furthermore, GLIMB includes five climate forcing parameters such as temperature, precipitation, long-term means-wind speed, relative humidity and solar radiation (Marzeion et al., 2020; Sakai & Fujita, 2017). Contrary, OGGM-VAS only includes the first two parameters, i.e. temperature and precipitation. It is difficult to determine whether the significant difference between the two models results from one of these two differences. If GLIMB's slow e-folding time is a result of using the energy balance method, it would be expected that James, which also follows a volume-area scaling and energy balance approach, would exhibit a similarly slow response time. The only e-folding time for James in Iceland shows, however, that the model behaves very similarly to OGGM-VAS. In fact, the two e-folding times are almost perfectly overlapping (see Iceland in Fig. 14 and Fig. 19 at a slope of 6.7% and ice thickness of 340m respectively, in a 75% volume loss scenario). While only one data point is not representative for interpretation (though the model's fast behaviour is expected for a volume-area scaling approach), it can act as an indication that the driving force behind GLIMB's slow response time must result from somewhere else. Unfortunately, we are not able to verify whether the slow e-folding time is the result of the three additional climate forcing parameters, as GLIMB is the only model in this thesis which accounts for them. It might be interesting to include simulations by Shannon et al. (2019) in future studies, as their model includes these additional parameters.
The second slowest model after GLIMB is Rounce, followed by Zekollari, Compagno and OGGM_v1.6. While Rounce tends to exhibit longer e-folding times, the latter three yield intermediate response times. All four models account for ice dynamics and are therefore expected to result in slower response times than volume-area scaling approaches. Comparing Rounce to OGGM_v1.6 is of interest as the former model is based on a hybrid model between PyGEM (Rounce, Hock, & Shean, 2020) and OGGM (Maussion et al., 2019), i.e. a previous version of OGGM_v1.6. Since Rounce obtains the ice dynamics from OGGM, the discrepancy in e-folding time might originate from the PyGEM component. Thus, the degree day method

in PyGEM could be one of the drivers behind the slower e-folding time for Rounce.
Similarities between Zekollari's and Compagno's e-folding time are expected as the former one corresponds to a 3d version of the latter. However, since simulations from the 3d version are only available for eight out of nineteen regions, an exact interpretation is difficult.
The last model analyzed in this thesis is Kraaijenbrink, which resulted in a fast e-folding time. Since this model is again based on a volume-area scaling approach, this fast reaction time is expected. However, uncertainties remain since only few regions are simulated with this model.

These deviations in model prediction are responsible for the described ranking differences in Section 5.1.2 , where Table A.1 projects slower response times compared to the ones in Table 6. Since the former table only utilizes models with a global coverage, it is limited to GLIMB, Rounce, Compagno and OGGM_v1.6. While the former two yield slow response times, the latter two predict intermediate response times. Hence, the mean between these four models will yield a response time between slow and intermediate, explaining the slower e-folding times in Table A.1 compared to Table 6.

Overall, regions simulated with models following a volume-area scaling approach react significantly faster to a new climate steady state, with GLIMB acting as exception. In contrast, models which include ice dynamics indicate a slower regional reaction to climate change. Considering that the inclusion of ice flow dynamics represents a more realistic approach, it is possible that the e-folding times obtained in this thesis from volume-area scaling models might be subject to underestimation.

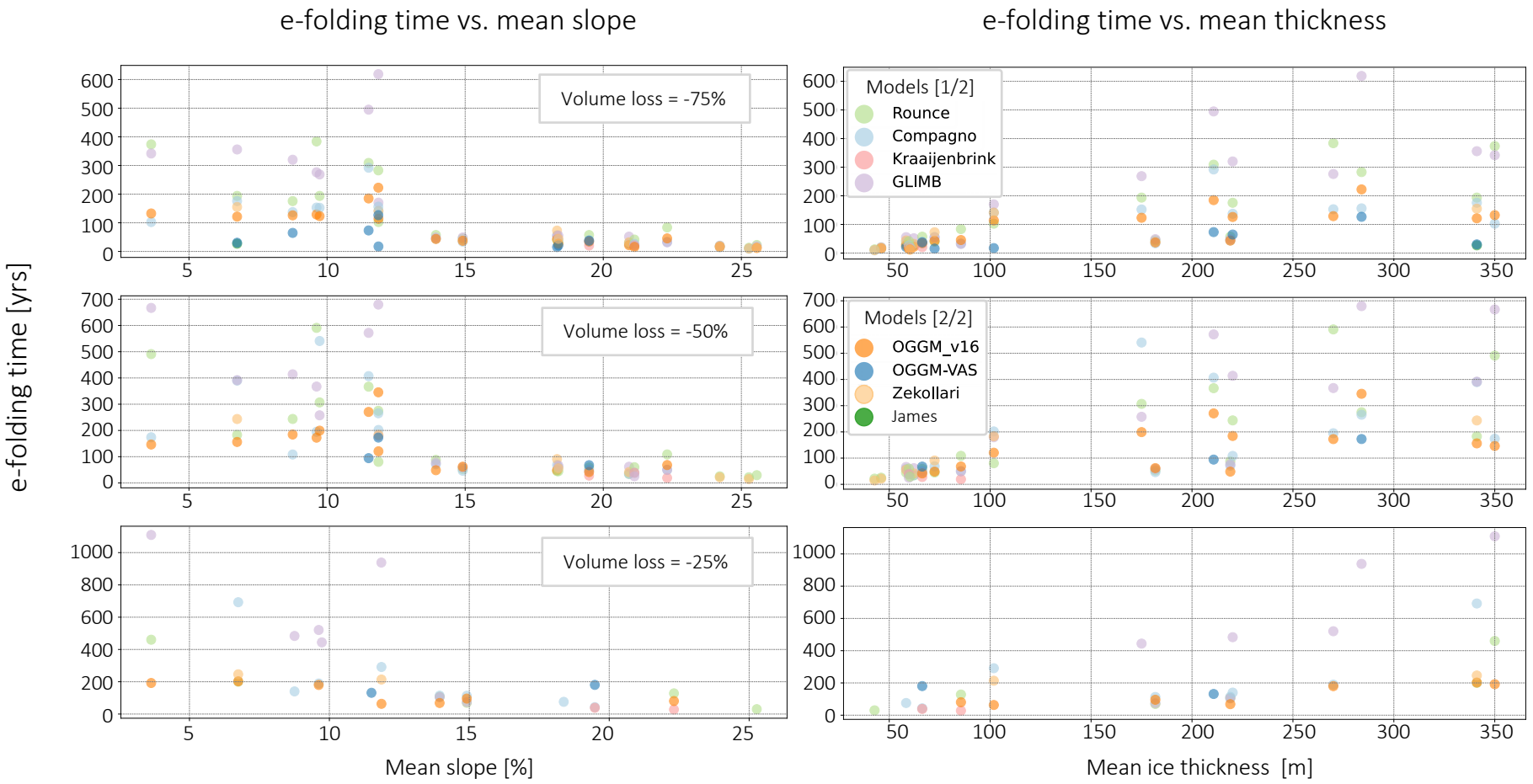

Figure 20: Left: Mean e-folding time is plotted with respect to the slope. Color coding corresponds to the different models. Note that the y-axis is different for all three subplots. **Right:** e-folding time for all models with respect to the mean ice thickness.

Table 7: Qualitative ranking of models by their regional e-folding time. Column *e-folding time* provides a measure of the relative response time compared to the other models. Models enclosed in brackets indicate difficulty in interpretation due to limited data availability (i.e. only few regions were simulated).

Qualitative model ranking throughout all volume loss scenarios		
e-folding time	**Model**	**Description**
Slow	GLIMB	Very slow response times for regions with mean slopes <13% throughout all volume loss scenarios and slow to intermediate response times for steeper regions.
Slow	Rounce	Similar to GLIMB as it also shows very slow response times for regions with a mean slope <13%. For most regions, Rounce yields the second slowest response time, directly after GLIMB.
Intermediate	(Zekollari)	Model data only available for 8/19 , making interpretation more challenging. Simulations yield response times similar to OGGM_v16 and Compagno. It appears that the model generates results within the range of slow to intermediate response times.
Intermediate	Compagno	Simulations yield an intermediate response time. For many regions, Compagno shows results faster than Rounce and GLIMB. Moreover, the model generates response times very similar to OGGM_v16.
Intermediate	OGGM_v1.6	Model results in intermediate response times which are very similar to Compagno. However, OGGM_v16 shows slightly faster response times.
Fast	OGGM-VAS	Fast response times for scenarios with large volume loss. Tends to be slower in case of little ice loss.
Fast	(Kraaijenbrink)	Model was simulated for three regions only, leaving limited scope for interpretation. Results indicate a very fast response time.
Fast	(James)	Model simulated the Iceland region only. Furthermore, a response time was solely obtained in case of a 75% volume loss, which shows a slightly faster response time than the one by OGGM-VAS in this region.

5.2.2 Comparison to Rounce et al. (2023)

As mentioned in Section 5.2, most studies focus on glacier simulations until the end of this century (e.g. Anderson and Mackintosh, 2012; Giesen and Oerlemans, 2013; Hirabayashi et al., 2013; Huss and Hock, 2015; Marzeion et al., 2012; Maussion et al., 2019; Radić et al., 2014; Rounce et al., 2023; Shannon et al., 2019; Slangen et al., 2012; Van de Wal and Wild, 2001; Zekollari et al., 2019). A recent publication by Rounce et al. (2023) expects glaciers to lose between 26% and 41% of their mass by the end of the century (relative to 2015), depending on the effective temperature increase. They estimate a corresponding sea level increase of 90mm to 154mm. These projections were simulated using the Rounce model (i.e. the hybrid model which utilizes PyGEM and OGGM). As described in Section 5.2.1, this model yields a relatively slow response time compared to other models. In fact, among the models which incorporate ice dynamics, it is the Rounce model which results in the slowest response times. Thus, due to this slower response time, regions will experience the projected volume loss over a longer time period. Therefore, it might be worth considering that the projected volume loss by Rounce et al. (2023) at the end of the century may be conservative, as other models suggest a faster response time. This finding coincides with the result by Zekollari et al. (in prep), displayed in Fig. 21. The figure shows the predicted volume loss under four SSP scenarios by the end of the century for GloGEM, OGGM_v1.6 and Rounce. Although the GloGEM model is not explicitly used in this thesis, simulations with the extended version GloGEMflow (Compagno) and GloGEMflow3d (Zekollari) are analyzed. The latter two models in the figure correspond to the same one as in this study. It is visible that, except for the GloGEM SSP1-2.6 scenario, Rounce projects a smaller volume loss by the end of the century. This difference is especially apparent between OGGM_v1.6 and Rounce for all SSP-scenarios. Additionally, if a glacier model simulates slower adjustment to climate change, the difference between various simulated climate scenarios will be smaller as well. Hence, the spread between the scenarios is smaller. This behaviour is visible in Fig. 21 as well, where the spread between the four different climate scenarios is smaller for the Rounce model compared to the others. Thus, the relatively slow response time for Rounce in this thesis compared to other glacier simulation models might be a partial explanation for the difference in projected volume loss as well as spread difference from Fig. 21.

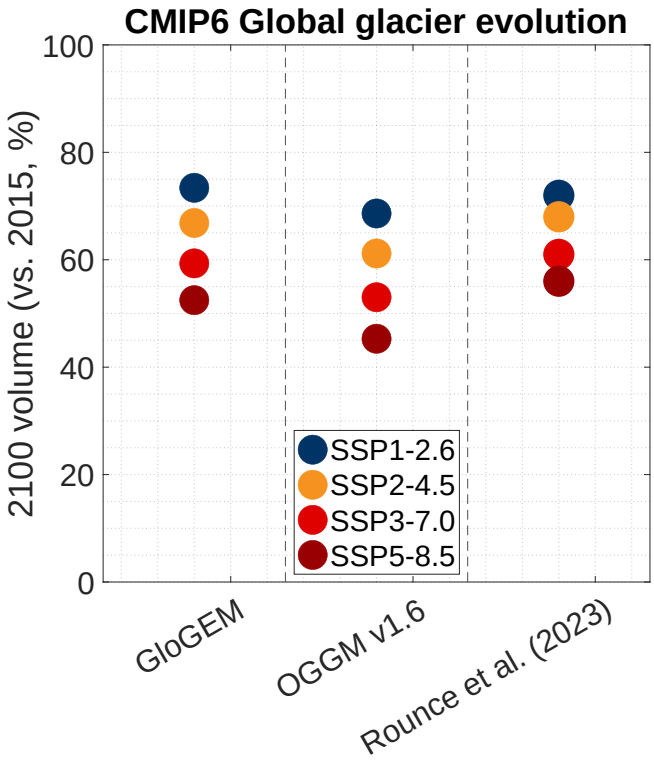

Figure 21: Unpublished graph by Zekollari et al. (in prep) which shows projected volume loss by the end of the century compared to 2015 for different SSP-scenarios and three models. The smaller spread as well as smaller projected volume loss with the Rounce model might be the result of its slower response time.

5.3 Random forest limitations

The random forest algorithm trained in this thesis can only rely on numerical values, which is the reason why the different models (e.g. GLIMB) are not included as feature. It is possible to use integers for each model instead (e.g. GLIMB would correspond to 1 and Compagno to 2), however, this method introduces a bias as it gives more weight to a model with a higher number, potentially overshadowing models with lower numbers. A common approach in machine learning to address this issue is to utilize the one-hot encoding method. (e.g. Goodfellow et al., 2016; Murphy, 2012). If one applies this method to solve the model-name issue, eight separate columns for each model get created. Each simulation will then have a value of zero or one in these additional columns, representing the presence or absence of each model. Hence, no overshadowing of models with a smaller number will occur. However, these added eight columns introduce further complexity to the decision tree structure, making it challenging to visually analyze the trees.

Furthermore, while the correlation between the features has not influenced the ranking of the two most important parameters (i.e. mean slope followed by mean ice thickness) described in Section 5.1.2, it is likely to have influenced the prediction quality. Hence, reducing this

correlation might be relevant for future applications with this algorithm.
Further improvements can be achieved by fine-tuning the algorithm's parameters. Here, no parameter tuning was applied in order to minimize the risk of overfitting. However, for future assessments, parameter-tuning could be considered to enhance the model's performance.

5.4 Stabilization time

Many simulations are removed during the filtering process of the e-folding time. The main driver behind the exclusion of data is the exponential fit, i.e. if a simulation does have a R^2 value being smaller than 0.95, it gets removed. This does not necessarily play an important role for large volume loss scenarios, since there are many available simulations which follow an exponential fit. However, as can be seen in previous figures (e.g. Fig. 14) some regions in case of a 25% volume loss do not show an e-folding time as there are no simulations left after filtering.
By examining the stabilization time instead, no exponential fit is applied in the filtering process as depicted in Fig. 11. Hence, the amount of simulations eliminated during the filtering process are significantly less. Table 8 presents the percentage of data removal at each step between e-folding and stabilization time. With 28.2%, the exponential fit plays by far the biggest role during the e-folding filtering process whereas the stabilization time is mostly affected by the removal of small relative volume change simulations, with 11.4 %. It is, however, important to note that the percentage of data being removed by the exponential fit threshold is not per se an indicative parameter to assess how much data is removed. This is due to the fact that some models performed many simulations in a specific region which did not adhere to an exponential fit, leading to a high number of eliminations for those regions and models. An example of such behaviour is visible for the OGGM-VAS model for Alaska in Fig. A.6. Due to the significant initial decrease in volume followed by a substantial mass gain, most of these simulations correspond to a poor exponential fit, leading to their exclusion. Therefore, the number of simulations removed is concentrated to a few regions for some specific models and it does not directly indicate that 28.2% of simulations are removed across all regions and simulations.
Still, as shown in Table 8, by using the stabilization time approach, the amount of eliminated data can be reduced by almost half, from 30.1% to 16.4%. This significant decrease does, however, not necessarily guarantee improved outcomes, as the results of the stabilization time need to be interpreted carefully.

Table 8: Total removed simulations during the three filtering steps for the e-folding and stabilization time. The 28.2% removal of the exponential fit needs to be interpreted with caution as it does not mean that every fourth simulation is removed in each region and for each model. This is because some few models performed almost all 80 simulations within a specific region with a poor exponential fit (e.g. see Fig. A.6), resulting in the exclusion of many simulations within said region.

Filtering step	**e-folding time** removed data [%]	**Stabilization time** removed data [%]
Small ΔV	1.9	11.4
Exponential fit	28.2	0
Steady state	0.01	5
Total	**30.1**	**16.4**

Determining the exact location of the stabilization time as shown in Fig. 6 is not straight forward. As depicted in this figure, the steady state time is located where a 2% volume change occurs, starting from the end of the time series. This location can be easily found for simulations which show little volume oscillations within a short time frame, as visible in Compagno's simulation in the left part of Fig. 22. On the contrary, models that result in strong oscillations, such as OGGM-VAS, shown in the right part of Fig. 22, reach the 2% volume change during these oscillation periods. This means that the stabilization time is massively overestimated since the points are located near the end of the total simulated years instead of the actual position, where the glacier reaches its state of equilibrium. Thus, the simulations have to be smoothed in order to reduce the oscillation effect. This, however, introduces follow-up problems. To mitigate the effects of the strong oscillations introduced by OGGM-VAS, it is important to use a sufficiently large window length for the smoothing function. This ensures that the rolling mean is calculated over a longer time span and hence, reduces the effect of strong volume variability. However, due to the increased length of the window, the stabilization time is underestimated for many cases since the true location is smoothed out. Hence, as the expected stabilization time is approached, the window length in this thesis is reduced to improve accuracy - leading in some cases, again, to overestimation.
Further uncertainties arise as the 2% change is obtained as the relative volume change between the initial volume and the volume at the end of the simulation. Therefore, simulations with little ice loss will be more significantly impacted by the 2% threshold, resulting in an overestimation of the stabilization time compared to large volume loss simulations. Due to these circumstances, the threshold is incrementally increased as the volume loss decreases. Obtaining this incremental increase is challenging: A significant increase results in underestimation whereas a minor increase leads to overestimation. Furthermore, although a specific set-up may be effective for one region or model, there is no guarantee that it will work equally well for all regions or models. Hence, the stabilization time results need to be very carefully interpreted, as there is a tendency of over- and underestimation.

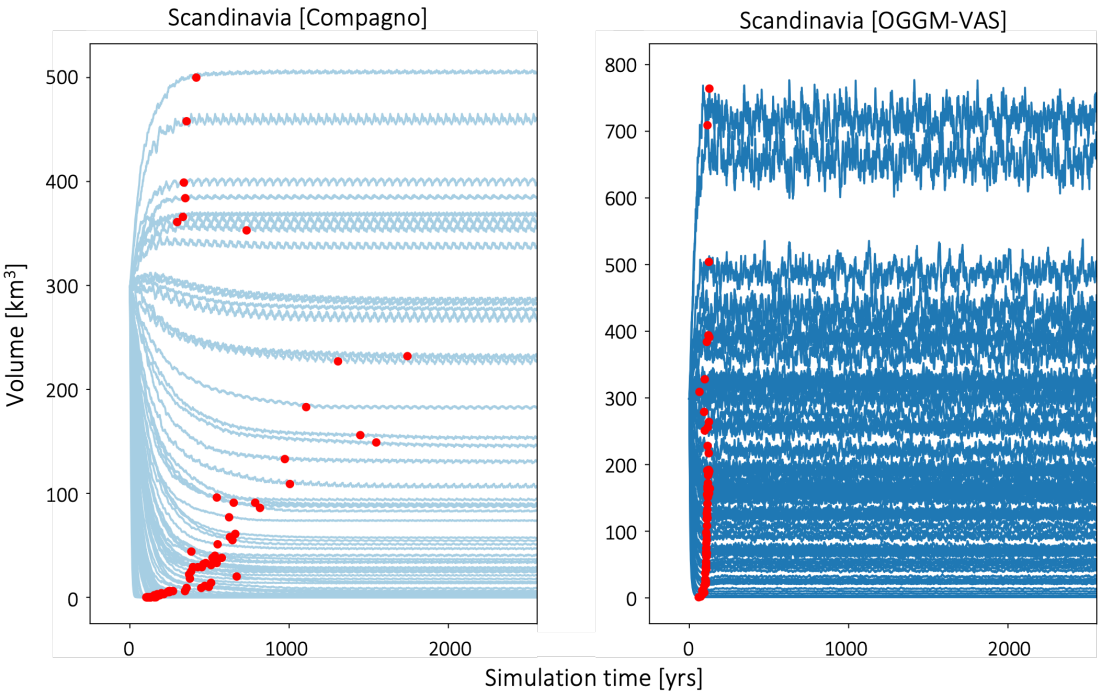

Figure 22: Left: Compagno's stabilization time points (red dots) obtained for Scandinavia. Simulations show little climate oscillations, i.e. little volume changes within short time periods. **Right:** Stabilization points for OGGM-VAS in Scandinavia. Strong volume changes within a short time frame are visible. A tendency of underestimation at a volume of 300 km^3 is visible, which is likely an artefact of the incremental threshold increase. Both plots are trimmed to show the first 2500 out of 5000 simulation years.

The regional stabilization time is displayed in Fig. 23 and the mean regional stabilization time can be seen in Fig. 24. Note that the former figure is sorted by increasing mean ice thickness whereas the latter by increasing mean slope, in order to facilitate comparison with the e-folding time overview figures (Fig. 14 and Fig. 19). The overall trend of fast and slow regions is very similar to the mean e-folding time in Fig. 19 and it becomes evident that the stabilization time is also highly influenced by the region's slope, which is what one would expect. Furthermore, since less data is removed during the filtering process, regions which did not have an e-folding time (e.g. South Asia East in a 25% volume loss scenario in Fig. 14) do now have a stabilization time. However, as previously explained, the stabilization time has to be interpreted carefully, especially for little volume loss scenarios as there is a risk of underestimation. This can be seen by comparing the three different loss scenarios in Fig. 24 with each other. There is an increase in stabilization time between a 75% and 50% loss which corresponds to the same behaviour which is visible for the e-folding time. However, in case of a 25% volume loss, the stabilization time seems to be faster, which is likely an artefact due to the incremental threshold increase.

The stabilization time was analyzed in order to remove less data. While this was achieved, the concept of using this approach needs to be refined in future projects as there is still large

induced uncertainty. However, as this method can reduce the amount of eliminated simulations by almost 50%, it might be a very interesting concept to pursue in future research.

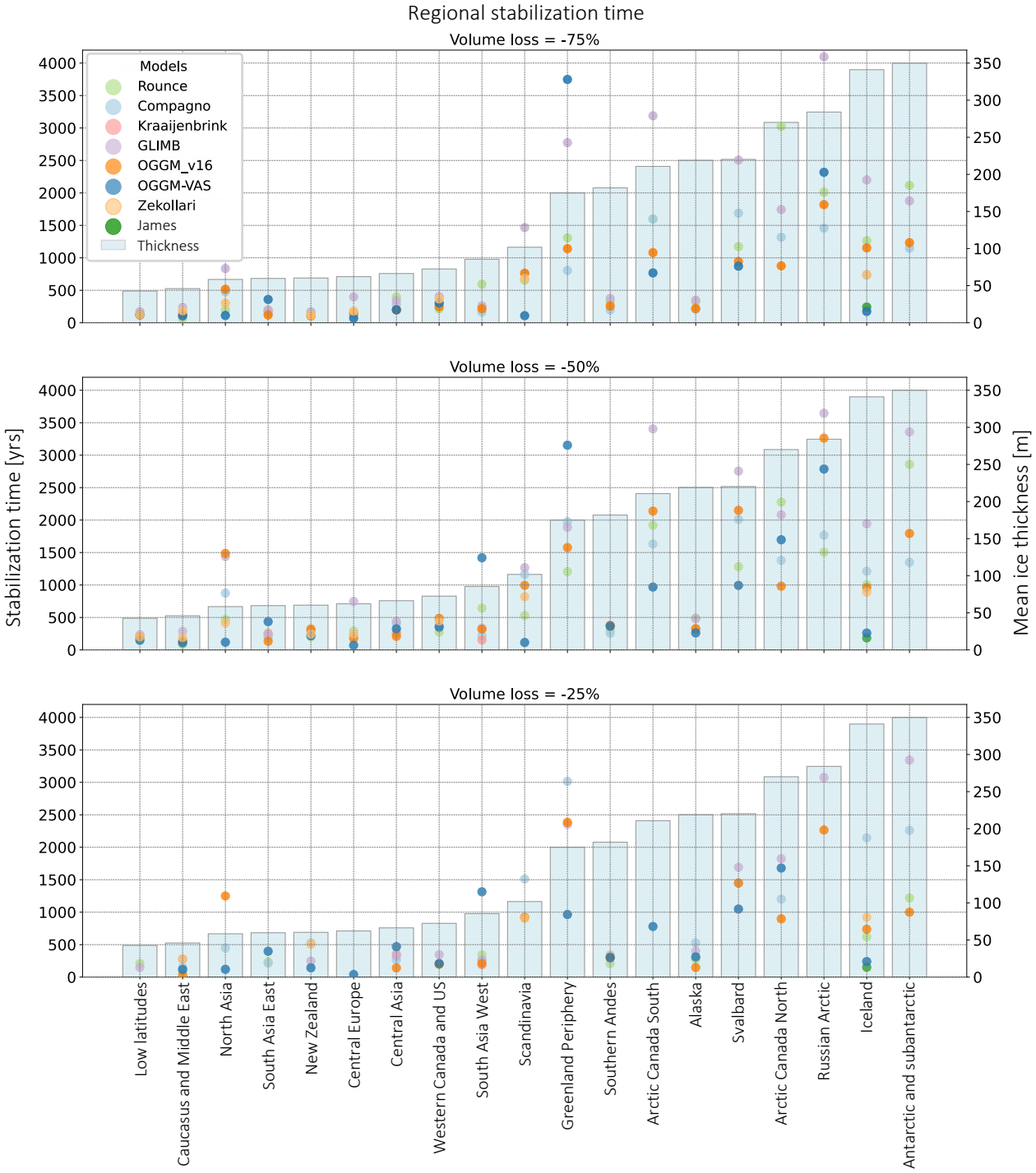

Figure 23: Stabilization time obtained for three different volume-loss scenarios, i.e. at a 75%, 50% and 25% loss. Colors correspond to the different models. Blue bars represent mean ice thickness within each region.

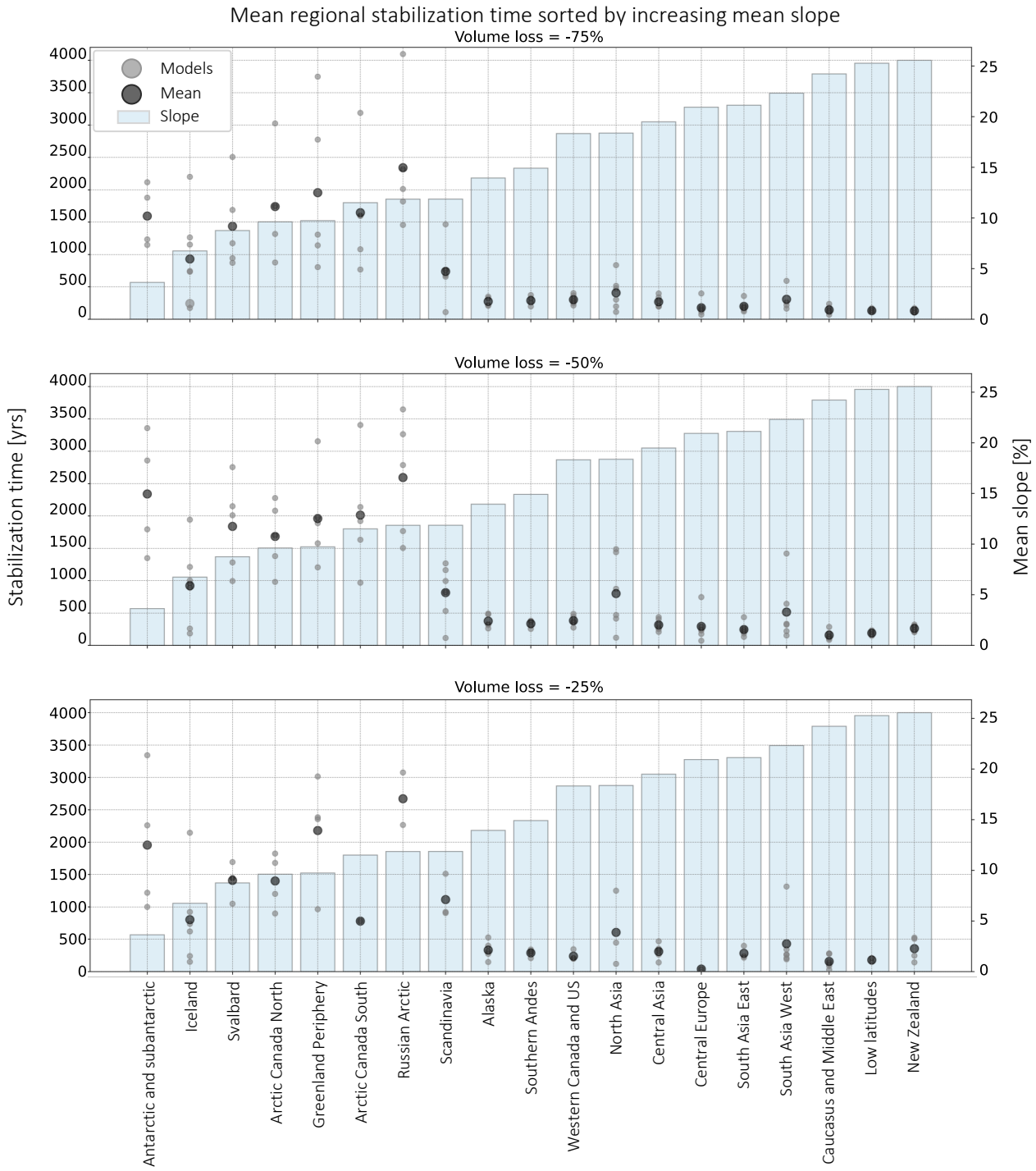

Figure 24: Mean regional stabilization time obtained for three different volume-loss scenarios, i.e. at a 75%, 50% and 25% loss. Grey dots represent models used for simulations. Black dots display mean regional stabilization time, obtained by calculating the mean between the different models per region. Blue bars represent mean regional slope.

6 Conclusion

In this study, the regional volume response time of glaciers to climate change is investigated through the e-folding time, corresponding to the time it takes for a glaciated region to reach $1 - e^{-1}$ (= ca. 63%) of its relative volume change. Furthermore, an additional concept that we refer to as the stabilization time is introduced, which complements the e-folding time by quantifying the time needed necessary for a glaciated region to reach a state of equilibrium.
The regional volume response time (hereafter typically referred to as response time) is derived from the output of eight different glacier evolution models that participated in the third phase of the Glacier Model Intercomparison Project (GlacierMIP3). These models simulated glacier advance or retreat for various climate scenarios over a long time span of 2000 to 5000 years. This time horizon allows glaciers to completely reach a steady state, which is different from simulations in the literature where glacier loss is usually simulated until the end of this century. In the latter case, glaciers are not in a state of equilibrium, which complicates determining the true response time and equilibrium state of a region.
To investigate the key driving parameters of the e-folding time, a 5-fold random forest algorithm is implemented. The algorithm is trained on the mean ice thickness, simulated volume change, mean glacier slope, the occurrence of calving and a latitudinal index. The decision trees' structure reveals that the mean glacier slope within a region has the most significant impact on the region's response time. More specifically, regions in which the mean slope is smaller than 13% yield slow response times, whereas areas with steeper slopes (above this threshold) are subject to significantly faster response times. Regions with gentle slopes typically contain large ice caps while those with a steeper slope are glacier-dominated. From this, we conclude that ice cap dominated regions take substantially longer to adjust to a new climate steady state than areas where only glaciers are present. Further important parameters that influence the response time are the mean ice thickness and the effective volume loss for a given climate change scenario. A distinction between slow and fast adapting areas to climate change can also be made based on the regions' latitude. High-latitude areas react to increasing temperature significantly slower than low-latitude ones.
Performing this comparison across different volume loss scenarios demonstrates that the ranking of regions in terms of e-folding time remains relatively consistent. Although the response time is influenced by the magnitude of volume loss, the overall order of regions based on their e-folding time remains similar.
We find, that the Earth's glaciated regions which adapt to climate change the fastest are the Low latitudes (regional volume response time of 10.8 ± 1.0 years for a 75% volume loss and 18.1 ± 3.4 years for a 50% loss), New Zealand (16.3 ± 2.4 years and 29.5 years, no uncertainty for the latter as e-folding time is obtained from one model only) and Caucasus & Middle East (17.6 ± 0.9 years and 23.4 ± 1.9 years). In contrast, the slowest areas are represented by the Russian Arctic (281.4 ± 88.5 years and 347.6 ± 87.4 years), Arctic Canada South (270.8 ± 70.1 and 342.1 ± 78.7 years) and Antarctic & subantarctic (237.7 ± 69.9 years and 369.6 ± 126.2 years). The models that performed the multi-millennial equilibrium simulations used in this thesis, from which the response time is calculated, show distinctively different glacier responses, both

in terms of magnitude and the rapidity of the response (i.e. the response time on which we focus here). Overall, models based on a volume-area scaling approach generally adjust faster to a new climate steady state, with GLIMB being an exception as it resulted in the slowest response time throughout all models tested in this study. GLIMB's unexpectedly slow response time might be due to the inclusion of additional climate forcing parameters when calculating the surface mass balance, which relies on an energy balance representation. However, since GLIMB is the only model analysed in this thesis which incorporates these additional parameters, it is difficult to draw a definitive conclusion. Comparing GLIMB's result to others that include additional climate forcing parameters (as opposed to most approaches that only rely on temperature and precipitation forcing) might be of interest for future studies.

In contrast to the volume-area scaling approaches, models incorporating ice dynamics project slower regional adaption to climate change. Considering the more realistic representation of ice dynamics in these models, it is, thus, possible that the response times obtained from volume-area scaling models might underestimate the true response times. Among the numerical models that incorporate ice dynamics, the simulations performed by the Rounce model (PyGEM-OGGM) have a tendency of yielding a slow adaption to climate change. Therefore, studies which use this model to assess glacier loss and sea level rise by the end of the century might predict a more conservative volume loss.

The filtering process applied in this study to obtain the e-folding time removes a considerable number of simulations based on the requirement of an exponential fit. This criterion has a larger impact on smaller volume loss scenarios, resulting in some regions having no estimated e-folding time. Since many simulations are removed by the e-folding filtering, a second method, referred to as the "stabilization time", is investigated. In the latter approach, the simulations do not have to follow an exponential fit, as only the time when a glacier reaches a state of equilibrium is of interest. Hence, since simulations which do not adhere to an exponential fit are not eliminated, the stabilization time approach reduces the amount of eliminated data by nearly half compared to the e-folding time approach. However, its results need careful interpretation as there is a tendency of underestimating the stabilization time, especially for simulations with a limited total volume loss. This underestimation is introduced in simulations with strong volume variations within a short timeframe, leading to a necessary smoothing of the simulations and thereby, introducing inaccuracies. Hence, future research could focus on refining the stabilization time concept to improve its interpretation and applicability.

All of the analyses in this thesis are based on regional glacier simulations. These simulations are derived from the sum of all individual glacier simulations within one region. Due to this summation, some specific response time features originating from individual glaciers are removed. It will therefore be interesting to further expand the work of this study and to quantify and explain the response time at the individual glacier level.

In summary, in this thesis, we for the first time analyze the invaluable GlacierMIP3 data archive to provide a unique insight in the regional response time of glaciers. Whereas our analysis, building on newly developed tools to describe the response of regions, quantified important differences in response time related to regional glacier characteristics and differences in model setup, further work will allow further exploring our newly introduced concepts and findings.

7 Acknowledgments

Thank you Dr. Harry Zekollari for this incredible research experience. Your guidance, constructive feedback, invaluable expertise and positive attitude throughout this project have helped me enormously.
Thank you Prof. Dr. Daniel Farinotti and Prof. Dr. Hansruedi Maurer for your valuable feedback and co-supervision of this work.
Thank you Codrut Diaconu for your helpful guidance on machine learning.
Thank you to my family for your support.
Thank you Irene for having endured my debugging complaints.

References

Anderson, B., & Mackintosh, A. (2012). Controls on mass balance sensitivity of maritime glaciers in the southern alps, new zealand: The role of debris cover. *Journal of Geophysical Research: Earth Surface*, *117*(F1).

Arendt, A. A., Echelmeyer, K. A., Harrison, W. D., Lingle, C. S., & Valentine, V. B. (2002). Rapid wastage of alaska glaciers and their contribution to rising sea level. *Science*, *297*(5580), 382–386.

Benn, D. I., & Lehmkuhl, F. (2000). Mass balance and equilibrium-line altitudes of glaciers in high-mountain environments. *Quaternary International*, *65*, 15–29.

Biau, G., & Scornet, E. (2016). A random forest guided tour. *Test*, *25*, 197–227.

Biemans, H., Siderius, C., Lutz, A., Nepal, S., Ahmad, B., Hassan, T., von Bloh, W., Wijngaard, R., Wester, P., Shrestha, A., et al. (2019). Importance of snow and glacier meltwater for agriculture on the indo-gangetic plain. *Nature Sustainability*, *2*(7), 594–601.

Bliss, A., Hock, R., & Radić, V. (2014). Global response of glacier runoff to twenty-first century climate change. *Journal of Geophysical Research: Earth Surface*, *119*(4), 717–730.

Boettinger, M., & Kasang, D. (2021). *The ssp scenarios*. Retrieved December 1, 2022, from https://www.dkrz.de/en/communication/climate-simulations/cmip6-en/the-ssp-scenarios

Breiman, L. (2001). Random forests. *Machine learning*, *45*, 5–32.

Christian, J. E., Koutnik, M., & Roe, G. (2018). Committed retreat: Controls on glacier disequilibrium in a warming climate. *Journal of Glaciology*, *64*(246), 675–688.

Compagno, L. (2022). *Process-based modelling for regional-to global-scale future impacts of glacier changes* (Doctoral dissertation). ETH Zurich.

Cuffey, K. M., & Paterson, W. S. B. (2010). *The physics of glaciers*. Academic Press.

Edwards, T. L., Nowicki, S., Marzeion, B., Hock, R., Goelzer, H., Seroussi, H., Jourdain, N. C., Slater, D. A., Turner, F. E., Smith, C. J., et al. (2021). Projected land ice contributions to twenty-first-century sea level rise. *Nature*, *593*(7857), 74–82.

Farinotti, D., Huss, M., Fürst, J. J., Landmann, J., Machguth, H., Maussion, F., & Pandit, A. (2019). A consensus estimate for the ice thickness distribution of all glaciers on earth. *Nature Geoscience*, *12*(3), 168–173.

Fischer, A., Olefs, M., & Abermann, J. (2011). Glaciers, snow and ski tourism in austria's changing climate. *Annals of Glaciology*, *52*(58), 89–96.

Giesen, R. H., & Oerlemans, J. (2013). Climate-model induced differences in the 21st century global and regional glacier contributions to sea-level rise. *Climate dynamics*, *41*, 3283–3300.

Glen, J. W. (1955). The creep of polycrystalline ice. *Proceedings of the Royal Society of London. Series A. Mathematical and Physical Sciences*, *228*(1175), 519–538.

Goodfellow, I., Bengio, Y., & Courville, A. (2016). *Deep learning*. MIT press.

Haeberli, W., & Weingartner, R. (2020). In full transition: Key impacts of vanishing mountain ice on water-security at local to global scales. *Water Security*, *11*, 100074.

Harrison, Raymond, C. F., Echelmeyer, K. A., & Krimmel, R. M. (2003). A macroscopic approach to glacier dynamics. *Journal of Glaciology*, *49*(164), 13–21.

Harrison, W., Elsberg, D., Echelmeyer, K., & Krimmel, R. (2001). On the characterization of glacier response by a single time-scale. *Journal of Glaciology*, *47*(159), 659–664.

Hausfather, Z. (2019). *Cmip6: The next generation of climate models explained*. Retrieved December 1, 2022, from https://www.carbonbrief.org/cmip6-the-next-generation-of-climate-models-explained/

Hirabayashi, Y., Zang, Y., Watanabe, S., Koirala, S., & Kanae, S. (2013). Projection of glacier mass changes under a high-emission climate scenario using the global glacier model hyoga2. *Hydrological Research Letters*, *7*(1), 6–11.

Hooke, R. L. (2019). *Principles of glacier mechanics*. Cambridge university press.

Huss, M., & Farinotti, D. (2012). Distributed ice thickness and volume of all glaciers around the globe. *Journal of Geophysical Research: Earth Surface*, *117*(F4).

Huss, M., & Hock, R. (2015). A new model for global glacier change and sea-level rise. *Frontiers in Earth Science*, *3*, 54.

Huss, M., & Hock, R. (2018). Global-scale hydrological response to future glacier mass loss. *Nature Climate Change*, *8*(2), 135–140.

Hutter, K. (1983). The application of the shallow-ice approximation. In *Theoretical glaciology* (pp. 256–332). Springer.

IPCC. (2013). Climate change 2013: The physical science basis. *Contribution of working group I to the fifth assessment report of the intergovernmental panel on climate change*.

IPCC. (2021). Climate change 2021: The physical science basis. *Contribution of Working Group I to the Sixth Assessment Report of the Inter- governmental Panel on Climate Change.*

Jóhannesson, T., Raymond, C., & Waddington, E. (1989). A simple method for determining the response time of glaciers. In *Glacier fluctuations and climatic change* (pp. 343–352). Springer.

Jordahl, K., den Bossche, J. V., Fleischmann, M., Wasserman, J., McBride, J., Gerard, J., Tratner, J., Perry, M., Badaracco, A. G., Farmer, C., Hjelle, G. A., Snow, A. D., Cochran, M., Gillies, S., Culbertson, L., Bartos, M., Eubank, N., maxalbert, Bilogur, A., … Leblanc, F. (2020). *Geopandas/geopandas: V0.8.1* (Version v0.8.1). Zenodo. https://doi.org/10.5281/zenodo.3946761

Kraaijenbrink, P. D., Bierkens, M., Lutz, A., & Immerzeel, W. (2017). Impact of a global temperature rise of 1.5 degrees celsius on asia's glaciers. *Nature*, *549*(7671), 257–260.

Leysinger Vieli, G.-M., & Gudmundsson, G. H. (2004). On estimating length fluctuations of glaciers caused by changes in climatic forcing. *Journal of Geophysical Research: Earth Surface*, *109*(F1).

Lüthi, M. P. (2009). Transient response of idealized glaciers to climate variations. *Journal of Glaciology*, *55*(193), 918–930.

Marzeion, B., Cogley, J. G., Richter, K., & Parkes, D. (2014). Attribution of global glacier mass loss to anthropogenic and natural causes. *Science*, *345*(6199), 919–921.

Marzeion, B., Hock, R., Anderson, B., Bliss, A., Champollion, N., Fujita, K., Huss, M., Immerzeel, W. W., Kraaijenbrink, P., Malles, J.-H., et al. (2020). Partitioning the uncertainty of ensemble projections of global glacier mass change. *Earth's Future*, *8*(7), e2019EF001470.

Marzeion, B., Jarosch, A., & Hofer, M. (2012). Past and future sea-level change from the surface mass balance of glaciers. *The Cryosphere*, *6*(6), 1295–1322.

Maussion, F., Butenko, A., Champollion, N., Dusch, M., Eis, J., Fourteau, K., Gregor, P., Jarosch, A. H., Landmann, J., Oesterle, F., et al. (2019). The open global glacier model (oggm) v1. 1. *Geoscientific Model Development*, *12*(3), 909–931.

Milner, A. M., Khamis, K., Battin, T. J., Brittain, J. E., Barrand, N. E., Füreder, L., Cauvy-Fraunié, S., Gíslason, G. M., Jacobsen, D., Hannah, D. M., et al. (2017). Glacier shrinkage driving global changes in downstream systems. *Proceedings of the National Academy of Sciences*, *114*(37), 9770–9778.

Murphy, K. P. (2012). *Machine learning: A probabilistic perspective*. MIT press.

Nan, F., Wang, J., & Saligrama, V. (2015). Feature-budgeted random forest. *International conference on machine learning*, 1983–1991.

NRCS, U. (2009). Part 630 hydrology national engineering handbook. *USDA-NRCS (United States Department of Agriculture-Natural Resources Conservation Service)*.

Nye, J. F. (1965). The frequency response of glaciers. *Journal of Glaciology*, *5*(41), 567–587.

Oerlemans, J. (2007). Estimating response times of vadret da morteratsch, vadret da palü, briksdalsbreen and nigardsbreen from their length records. *Journal of Glaciology*, *53*(182), 357–362.

Oerlemans, J., Anderson, B., Hubbard, A., Huybrechts, P., Johannesson, T., Knap, W., Schmeits, M., Stroeven, A., Van de Wal, R., Wallinga, J., et al. (1998). Modelling the response of glaciers to climate warming. *Climate dynamics*, *14*(4), 267–274.

Oerlemans, J. (2001). *Glaciers and climate change*. CRC Press.

Oerlemans, J. (2018). Modelling the late holocene and future evolution of monacobreen, northern spitsbergen. *The Cryosphere*, *12*(9), 3001–3015.

Patro, E. R., De Michele, C., & Avanzi, F. (2018). Future perspectives of run-of-the-river hydropower and the impact of glaciers' shrinkage: The case of italian alps. *Applied Energy*, *231*, 699–713.

Pfeffer, W. T., Arendt, A. A., Bliss, A., Bolch, T., Cogley, J. G., Gardner, A. S., Hagen, J.-O., Hock, R., Kaser, G., Kienholz, C., et al. (2014). The randolph glacier inventory: A globally complete inventory of glaciers. *Journal of glaciology*, *60*(221), 537–552.

Radić, V., Bliss, A., Beedlow, A. C., Hock, R., Miles, E., & Cogley, J. G. (2014). Regional and global projections of twenty-first century glacier mass changes in response to climate scenarios from global climate models. *Climate Dynamics*, *42*, 37–58.

Radić, V., & Hock, R. (2011). Regionally differentiated contribution of mountain glaciers and ice caps to future sea-level rise. *Nature Geoscience*, *4*(2), 91–94.

Roe, G. H., & Baker, M. B. (2014). Glacier response to climate perturbations: An accurate linear geometric model. *Journal of Glaciology*, *60*(222), 670–684.

Roe, G. H., & O'Neal, M. A. (2009). The response of glaciers to intrinsic climate variability: Observations and models of late-holocene variations in the pacific northwest. *Journal of Glaciology*, *55*(193), 839–854.

Rounce, D. R., Hock, R., Maussion, F., Hugonnet, R., Kochtitzky, W., Huss, M., Berthier, E., Brinkerhoff, D., Compagno, L., Copland, L., et al. (2023). Global glacier change in the 21st century: Every increase in temperature matters. *Science*, *379*(6627), 78–83.

Rounce, D. R., Hock, R., & Shean, D. E. (2020). Glacier mass change in high mountain asia through 2100 using the open-source python glacier evolution model (pygem). *Frontiers in Earth Science*, *7*, 331.

Rounce, D. R., Khurana, T., Short, M. B., Hock, R., Shean, D. E., & Brinkerhoff, D. J. (2020). Quantifying parameter uncertainty in a large-scale glacier evolution model using bayesian inference: Application to high mountain asia. *Journal of Glaciology*, *66*(256), 175–187.

Sakai, A., & Fujita, K. (2017). Contrasting glacier responses to recent climate change in high-mountain asia. *Scientific reports*, *7*(1), 1–8.

Schaefli, B., Manso, P., Fischer, M., Huss, M., & Farinotti, D. (2019). The role of glacier retreat for swiss hydropower production. *Renewable energy*, *132*, 615–627.

Schuster, L. (2020). Response time sensitivity of glaciers using the open global glacier model. *Master Thesis. Universität Innsbruck*.

Shannon, S., Smith, R., Wiltshire, A., Payne, T., Huss, M., Betts, R., Caesar, J., Koutroulis, A., Jones, D., & Harrison, S. (2019). Global glacier volume projections under high-end climate change scenarios. *The Cryosphere*, *13*(1), 325–350.

Slangen, A., Katsman, C., Van de Wal, R., Vermeersen, L., & Riva, R. (2012). Towards regional projections of twenty-first century sea-level change based on ipcc sres scenarios. *Climate dynamics*, *38*, 1191–1209.

Strobl, C., Boulesteix, A.-L., Kneib, T., Augustin, T., & Zeileis, A. (2008). Conditional variable importance for random forests. bmc bioinformatics 9 (307).

Van de Wal, R., & Wild, M. (2001). Modelling the response of glaciers to climate change by applying volume-area scaling in combination with a high resolution gcm. *Climate Dynamics*, *18*, 359–366.

Veh, G., Korup, O., & Walz, A. (2020). Hazard from himalayan glacier lake outburst floods. *Proceedings of the National Academy of Sciences*, *117*(2), 907–912.

WCRP. (2022). *Wcrp coupled model intercomparison project (cmip)*. Retrieved December 1, 2022, from https://www.wcrp-climate.org/wgcm-cmip

Welling, J. T., Árnason, Þ., & Ólafsdottír, R. (2015). Glacier tourism: A scoping review. *Tourism Geographies*, *17*(5), 635–662.

Zekollari, H., Huss, M., & Farinotti, D. (2019). Modelling the future evolution of glaciers in the european alps under the euro-cordex rcm ensemble. *The Cryosphere*, *13*(4), 1125–1146.

Zekollari, H., Huss, M., & Farinotti, D. (2020). On the imbalance and response time of glaciers in the european alps. *Geophysical Research Letters*, *47*(2), e2019GL085578.

Zekollari, H., Huss, M., Maussion, F., Schuster, L., Rounce, D., Compagno, L., Hugonnet, R., Marzeion, B., Seyedhamidreza, M., Champollion, N., & Farinotti, D. (in prep). Global glacier evolution under cmip6 scenarios and the role of glacier-specific observations. *[Paper in preparation]*.

Zekollari, H., & Huybrechts, P. (2015). On the climate–geometry imbalance, response time and volume–area scaling of an alpine glacier: Insights from a 3-d flow model applied to vadret da morteratsch, switzerland. *Annals of Glaciology*, *56*(70), 51–62.

A Appendix

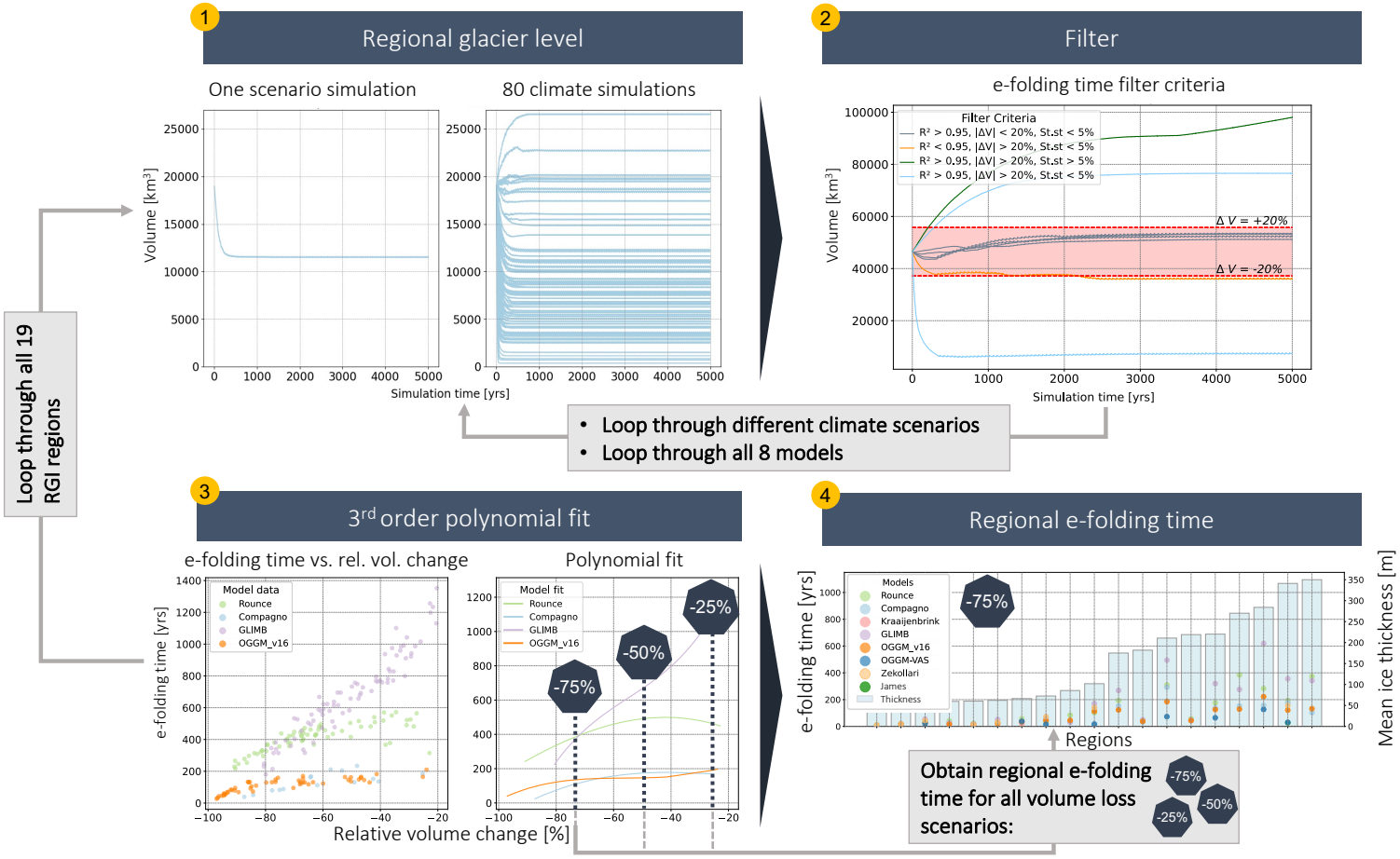

Figure A.1: Flowchart of the applied process for obtaining the regional e-folding time. Step 1: Simulations on a regional glacier volume level are used as underlying data. Step 2: Some simulations get filtered out, described by a filter criteria. The two steps are repeated for all different climate scenario simulations and different models. Step 3: e-folding time gets plotted with respect to its relative volume change in the left plot. Right plot shows polynomial fit through the data points. e-folding times are now obtained at a 75%, 50% and 25% volume loss. This part is done for all regions, resulting in the plot in Step 4.

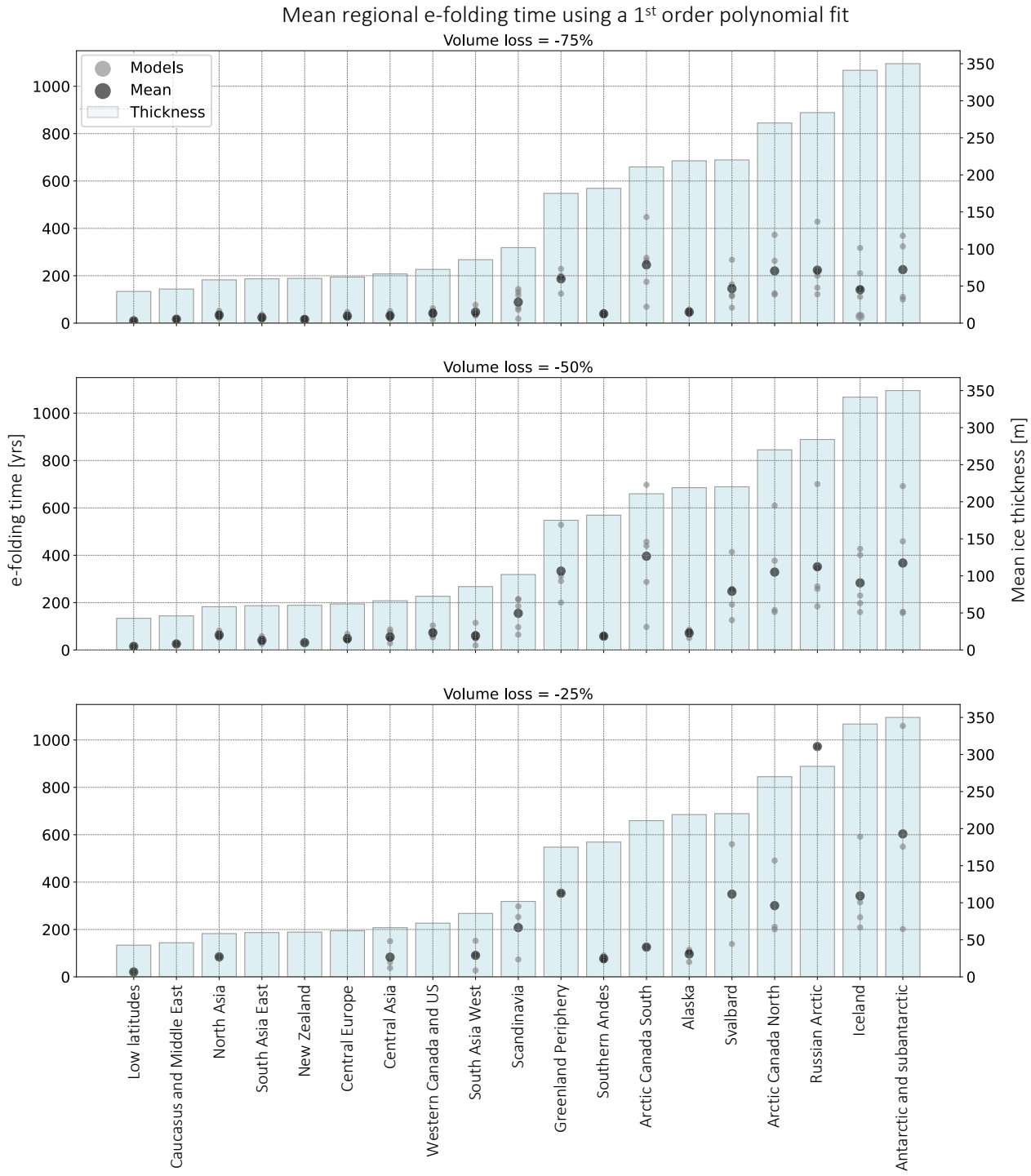

Figure A.2: Mean regional e-folding time obtained by using a linear fit instead of the 3^{rd} order polynomial from Fig. 14. The choice of fitting has little influence on the regional e-folding time.

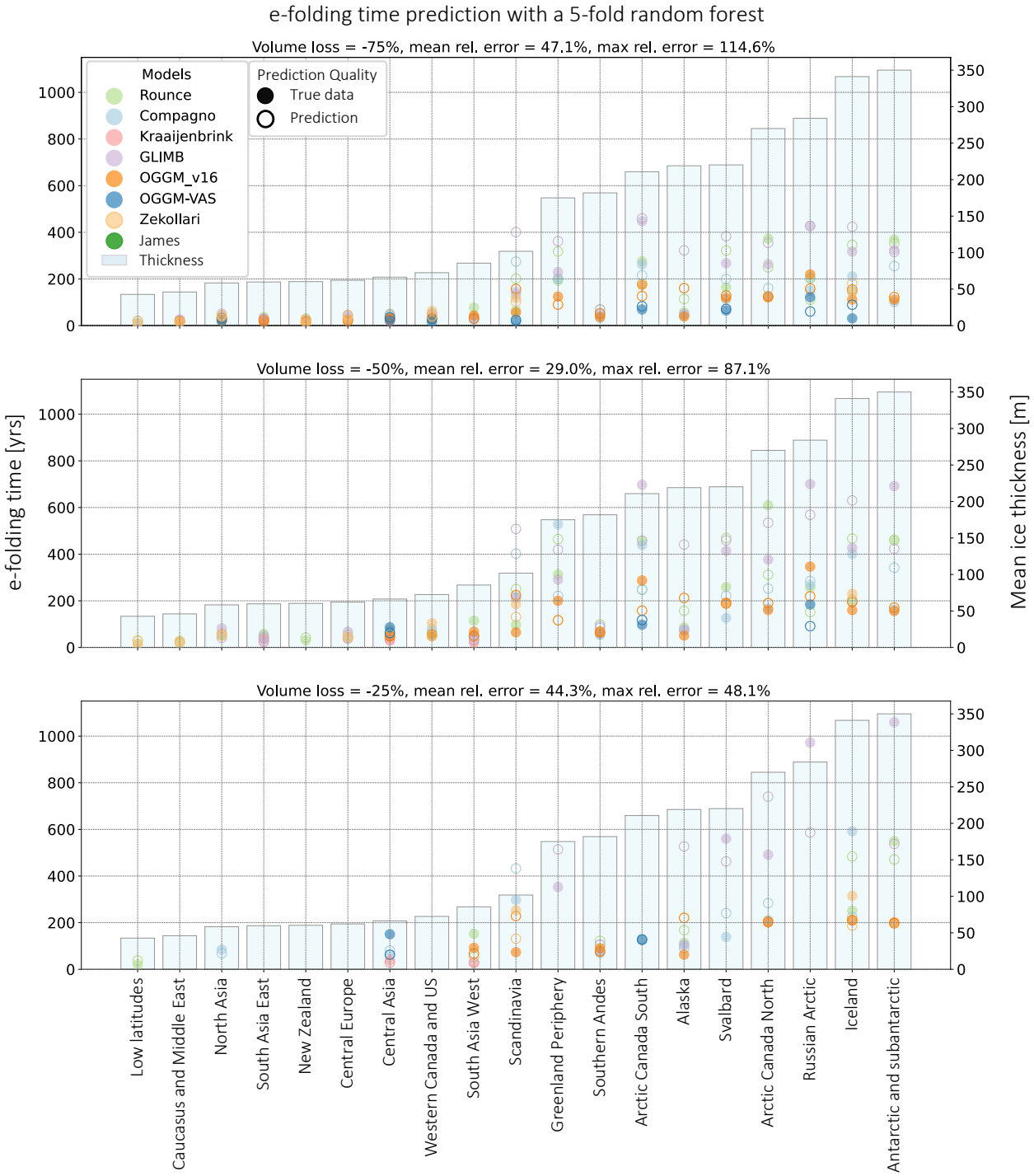

Figure A.3: Regional e-folding time predicted with a 5-fold random forest algorithm. Filled circles represent true e-folding time for a specific region and volume loss. Outlined circles correspond to predicted e-folding time. Color code shows the different models. Data is sorted by increasing ice thickness (blue bars).

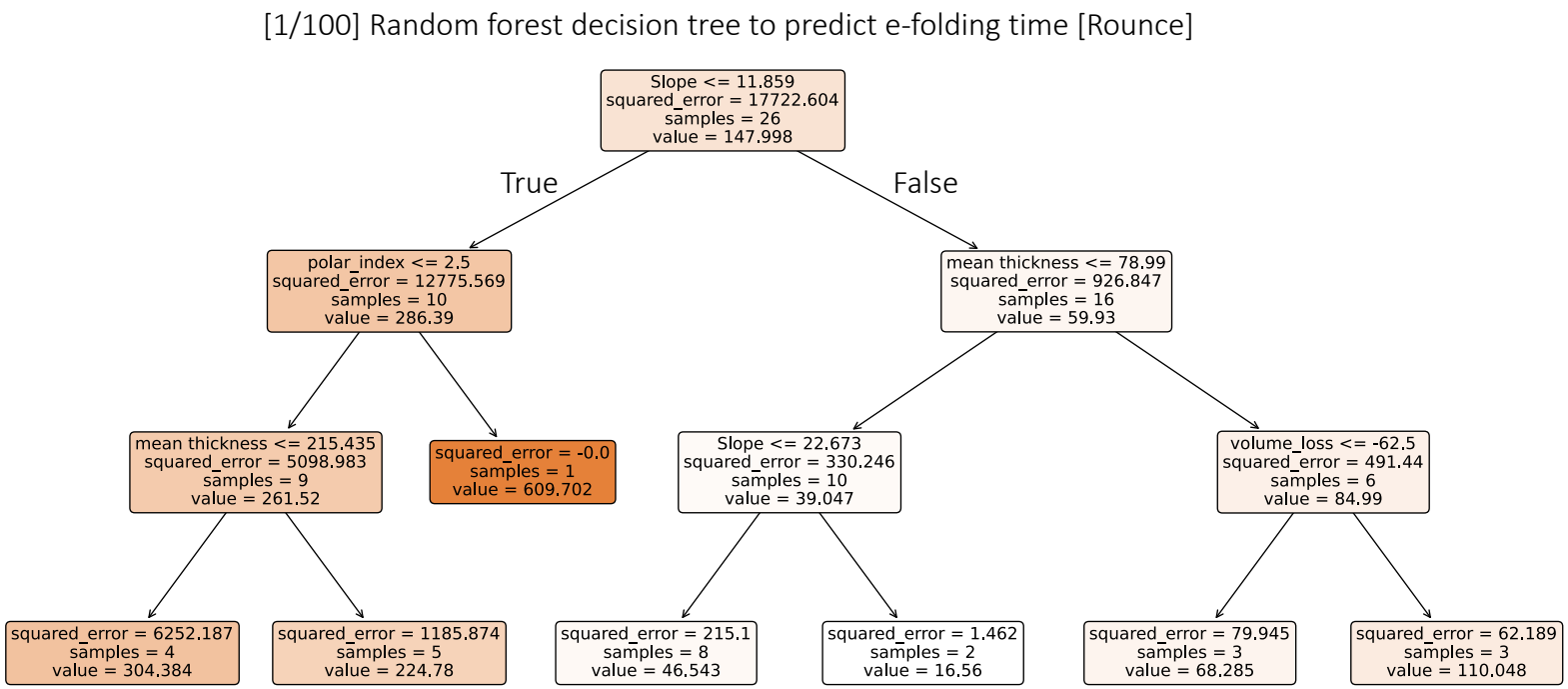

Figure A.4: Example Decision tree created by the random forest when trained on Rounce. Tree is limited to a depth of three nodes only for illustration purposes, i.e the algorithm was not limited to any depths in this thesis. The features (e.g. Slope in first node) show the algorithm's set threshold. Color coding corresponds to the estimated e-folding time on each node: A longer e-folding time (named *value* in the tree) is represented by a darker color. Note that this tree only corresponds to one out of hundred trees in a specific subsample.

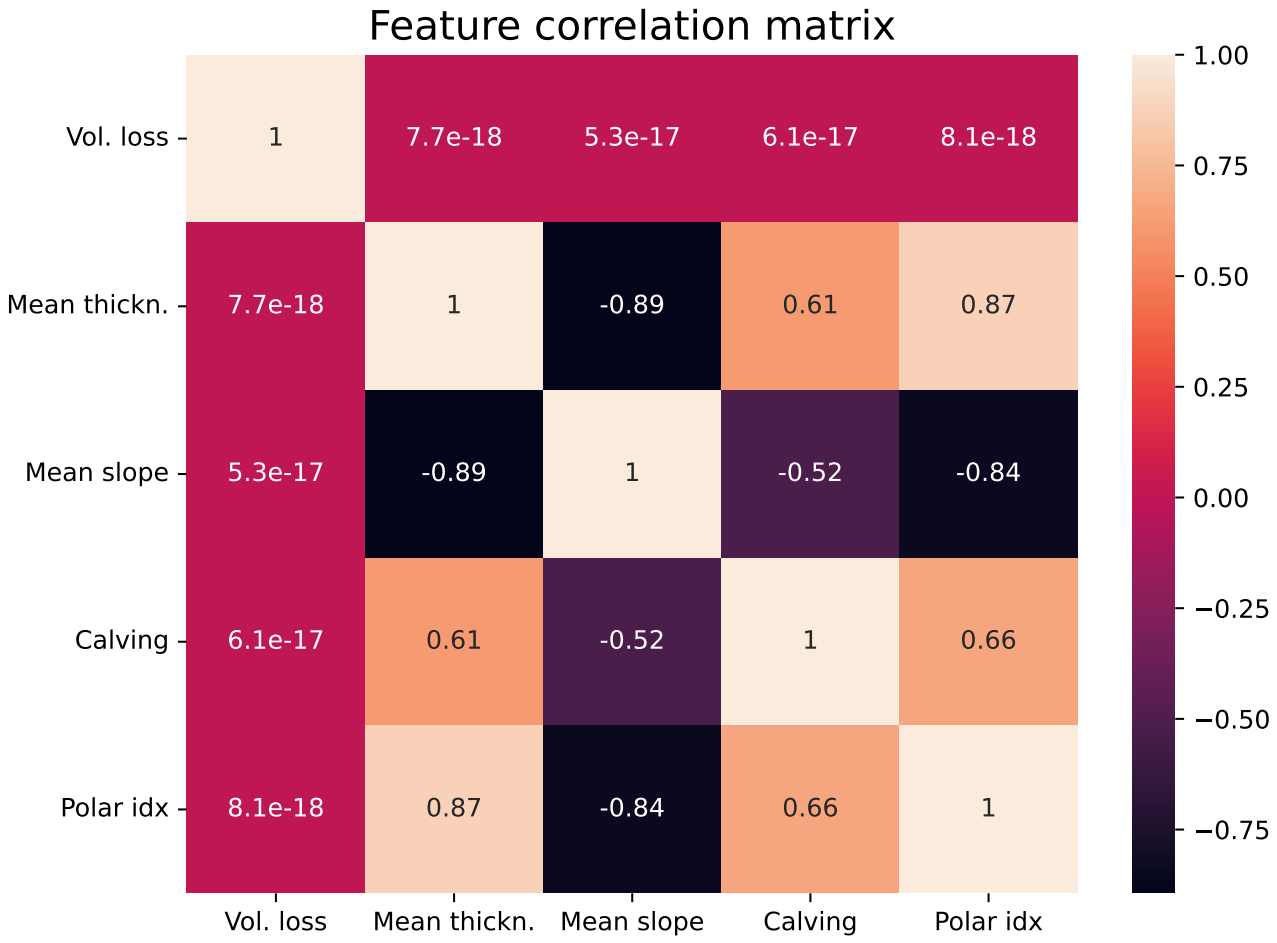

Figure A.5: Correlation matrix of features used in the random forest.

Table A.1: Mean regional e-folding time for a 75% volume loss scenario. Regions are sorted by increasing e-folding time. Only models which simulated all regions were used i.e. e-folding time is derived from Compagno, Rounce, OGGM_v16 and GLIMB.

75% volume loss scenario [Only global coverage models included]	
Region	e-folding time [yrs]
Low latitudes	11.2 ± 1.6
New Zealand	17.6 ± 3
Caucasus and Middle East	17.6 ± 1.3
South Asia East	26.1 ± 5.5
Central Europe	32.5 ± 6.6
North Asia	38.7 ± 6.3
Central Asia	41.2 ± 5.5
Southern Andes	41.2 ± 3.3
Alaska	48.3 ± 3.2
Western Canada and US	48.4 ± 4.1
South Asia West	48.6 ± 12.1
Scandinavia	132 ± 15.1
Greenland Periphery	184.5 ± 31.6
Svalbard	189.7 ± 44.7
Iceland	211.7 ± 50.5
Arctic Canada North	235.5 ± 59
Antarctic and subantarctic	237.7 ± 69.9
Russian Arctic	320.1 ± 102.9
Arctic Canada South	320.2 ± 64.4

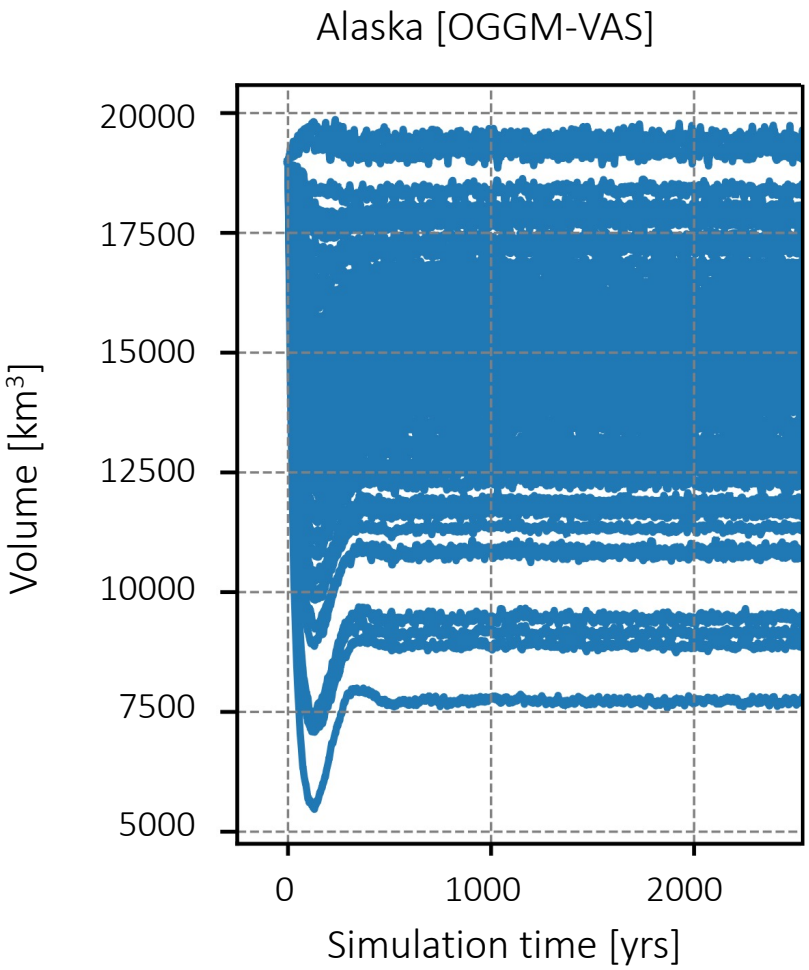

Figure A.6: Simulations by OGGM-VAS for Alaska show strong dip during the first 100 years, followed by an increase in volume afterwards. Due to this behaviour, many of these simulations (in this plot) do have a poor exponential fit, and are therefore excluded during the exponential fit filtering.

Eidgenössische Technische Hochschule Zürich
Swiss Federal Institute of Technology Zurich

Declaration of originality

The signed declaration of originality is a component of every semester paper, Bachelor's thesis, Master's thesis and any other degree paper undertaken during the course of studies, including the respective electronic versions.

Lecturers may also require a declaration of originality for other written papers compiled for their courses.

I hereby confirm that I am the sole author of the written work here enclosed and that I have compiled it in my own words. Parts excepted are corrections of form and content by the supervisor.

Title of work (in block letters):

Unhealthy and out of shape: Deciphering the slow response of glaciers to climate change

Authored by (in block letters):
For papers written by groups the names of all authors are required.

Name(s):	**First name(s):**
Wettstein	Christian

With my signature I confirm that

- I have committed none of the forms of plagiarism described in the 'Citation etiquette' information sheet.
- I have documented all methods, data and processes truthfully.
- I have not manipulated any data.
- I have mentioned all persons who were significant facilitators of the work.

I am aware that the work may be screened electronically for plagiarism.

Place, date	**Signature(s)**
Dietikon, 20.07.2023	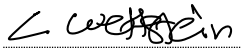

For papers written by groups the names of all authors are required. Their signatures collectively guarantee the entire content of the written paper.